Science
AAAS

Supplementary Materials for

Genetic diversity loss in the Anthropocene

Moises Exposito-Alonso *et al*.

Corresponding author: Moises Exposito-Alonso, moisesexpositoalonso@gmail.com

Science **377**, 1431 (2022)
DOI: 10.1126/science.abn5642

The PDF file includes:

Other Supplementary Material for this manuscript includes the following:

Table of contents

SUPPLEMENTAL MATERIALS & METHODS

I. Background on species biodiversity and biogeography

I.1 Theoretical models of biodiversity

The frequency or abundance of different species are often visualized with two types of histograms: Preston plot (Fig. S1, left), with x-axis the logarithm of abundance bins and y-axis the number of species at given abundance. Alternatively, the Whittaker plot (Fig. 1, right), with x-axis the species list ranked by their order of abundance (i.e. from common to rare), and in the y-axis the logarithm of % relative abundance. These are both aiming to describe distributions that are very uneven, as a key insight of species abundance distributions is the "commonness of rarity". Most species have low abundance and just a few are at high abundance.

The 20th century showed intense modeling of these distributions (Fig. S2, see summaries of early models in (*34*) or (*35*, *36*)). The models that have become most useful include Fisher's log-series distribution (*37*), Preston's log-normal distribution (*38*), and Hubbells' UNTB (*34*).

Fisher's log series assumes that species abundances in the community are independent identically distributed variables, sampling is a Poisson process, sampling is done with replacement, or the fraction sampled is small enough to approximate a sample with replacement. Here,

$$S_n = \frac{\alpha x^n}{n},$$

where x is a constant $x \in [0, 1]$ related to the sample dataset (typically close to 1), $x = \frac{N}{\alpha+N}$, and α is a new constant term (ecosystem-specific) that is used as a measure of biodiversity. Fisher proposed the number of species could be estimated as:

$$S = \alpha \times log\left(1 + \frac{N}{\alpha}\right).$$

Preston (*38*) posed that the skewness of previous proposals is due to lack of sampling. With little data, common species are collected sooner, but with more abundant sampling, the rarest species are also well-sampled and have abundances well above 0. Preston then proposed that the octaves (bins of doubling abundance) follow a normal distribution, making the raw abundance log-normal distributed. Given S_0 is the number of species in the model octave of abundance and a variance composite of the log-Normal σ^2, the number of species per abundance (octave) bin R (=*log(n)*) is:

$$S_R = S_0 e^{-R^2/2\sigma^2}.$$

The Unified Neutral Theory of Biodiversity (UNTB) by Hubbell (*34*) takes a stochastic approach of a community with immigrants, extinctions, and speciation in continuous dynamics. Interestingly, the UNTB's key parameter, θ, coincides with Fisher's α, as the log-series is a limiting case of UNTB. Hubbell's discovery was that $\alpha=2J_m v$, where J_m is the size of the external metacommunity that provides migrants of species to the focal community, and v is the speciation rate. Alonso and McKane (*39*) derived the so-called

Metacommunity Zero-Sum Multinomial (MZSM) distribution from the UNTB. In practice, both distributions have almost-identical fits (lines completely overlapping in Fig. S2).

I.2 Metric of species diversity

Although a number of metrics exist to measure species diversity, such as the Shannon index, $H' = -\sum_{i=1}^{S} P_i log P_i$ (with *Pi* the relative proportions of species abundances) or Fisher's non-dimensional α parameter, the study of species abundances and area relationships has focused on species richness *S*, that is, the total number of species in a given location or area. Below we therefore focus on species richness.

I.3 Biogeography of species and extinction.

SAD and SAR connection

Due to many species being rare, it is expected that as researchers sample an area, the most common species will be sampled first, and as the area studied increases, more and more species will be discovered. This is thought to happen following a power law relationship, where the number of species in that area S_A increases with the sampled area A, with scaling *z* (slope in a log-log plot), and with a constant *c*:

$$SAR(A) = cA^z.$$

Preston (*20*) derived theoretically that from a log-normal series, one would expect *z*=0.27, under a number of assumptions (Fig. S3). This has been empirically shown to be close to reality (*15*, *20*), although there is some variation across ecosystems and spatial scales.

I.4 Estimating extinction of species from the species area relationship

The first estimates of species extinction used the SAR relationship. Given a reduction of ecosystem area, *A*, by an area of *a* (*16*, *40*). If these areas, as well as the SAR scaling, *z*, are known, then one can predict the number of species in the future as:

$$S_{\text{now}} - S_{\text{fut}} = cA_{\text{now}}^z - cA_{\text{fut}}^z,$$

However, we are normally interested in the fraction of species that will go extinct X_s so we can take the ratio:

$$X_s = \frac{S_{\text{now}} - S_{\text{fut}}}{S_{\text{now}}} = 1 - \frac{cA_{\text{fut}}^z}{cA_{\text{now}}^z} = 1 - \left(\frac{A_{\text{fut}}}{A_{\text{now}}}\right)^z.$$

II. Population genetics models and the site frequency spectrum.

II.1 The Wright-Fisher model and the site frequency spectrum

Statisticians and population geneticists from the 20th century, Wright and Fisher, built a simple statistical model of evolution of a population. It assumes that each generation a population of *N* monoecious (hermaphrodite) individuals mate randomly to create a new generation of *N* individuals and then immediately die so that only *N* individuals remain in the population at any given time. This random sampling process causes the frequency of a variant in one generation to possibly differ from its frequency in the previous generation—a process known as genetic drift.

When a nucleotide mutation or variant (e.g. ACG**A**A → ACG**T**A) emerges by a random process of, for instance, DNA replication error, it will first be in 1/*N* individuals (if we consider these diploid, 1/2N chromosomes). Through random sampling that **T** mutation may be lost, stay at the same frequency, or randomly move to higher frequency. Although rarely, just by chance, the mutation may reach 100% frequency. This results in a "commonness of rarity" when looking at mutations in a population, as we have seen in previous sections for species. Since these genetic drift dynamics affect all mutations genome-wide, we therefore expect the majority of mutations to be absent, or rare, and only a much smaller proportion of variants to be at moderate or high frequencies.

The site frequency spectrum (SFS) refers to the distribution of frequencies of variants in a population. This is the number of sites at which we observe a variant at frequency *q* in a sample of *n* individuals. To derive the expected SFS distribution, we turn to Kingman's Coalescent (*41*). Both models describe the same ideal population of random mating, constant population size, and mutations emerging at a low rate and drifting in frequency. But while the Wright-Fisher model describes the dynamics of a whole population forward-in-time, the Kingman's Coalescent describes the genealogy of a sample of individuals from a population, going backward in time. By building a model around the individuals that are sampled or that survived, rather than of an entire population, the Coalescent provides a simpler way to derive expectations in small populations or in cases, for example here, where a limited sample of genomes are sequenced. Using the Coalescent (see (*42*) for details), one obtains that the expected number of mutations of a given abundance, *n*, is inversely related to their frequency, *q*:

$$M_n = c\frac{1}{q}$$

for some constant c that depends on the mutation rate and the population size. This SFS from population genetics theory is remarkably similar to the Species Abundance Relationship. In fact, Fisher himself (*18*) derived an expression similar to the above.

Rearranging terms, one can see this is a constrained version of the log-series Probability Mass Function (PMF), which Fisher also proposed for the distribution of species abundances (*37*). Below, one can graphically see the similarities (Fig. S4):

Keeping the abundance, n, constant (and low), when the number of individuals $N \to \infty$, we know that the constant x from Fisher's SAD approaches 1, $x = \frac{N}{N+\alpha} \to 1$. Then, we can rewrite the number of species at any given abundance (S_n) as:

$$S_n = \alpha\frac{(\frac{N}{\alpha+N})^n}{n} = \alpha\frac{1^n}{n} = c\frac{1}{n} = M_n$$

So both have the same form as the log series PMF: $f(k) = \frac{-1}{ln(1-p)}\frac{p^k}{k}$ when $p \to 1$. In the next section we will see that the constants of the SAD and the SFS are proportional to species and mutation diversity, although the Site Frequency Spectrum (SFS) is a specific case of SAD. One can also see that because the constant in the SFS is the population scaled mutation rate, $c = \theta = Ne\mu$, and Fisher's $\alpha \approx \theta$ for large N.

II.2 Metrics of genetic diversity

In population genetics, multiple measurements of genetic diversity have been put forward. The most straightforward is the allelic richness, also number of mutations, or also called the number of segregating sites. Segregating sites, *M*, is the direct equivalent of the species richness*, S*, and it depends on the number of samples used and length of DNA sequence explored (Note: we use the non-standard notation, *M*, as the standard in population genetics is *S* [for segregating sites] but this is already in use for species richness. We then use *M* for mutations and *S* for species). This metric can also be thought of as the area under the curve of the SFS. Two other metrics that describe the SFS but that aim to be sequence-length- and individual independent are Watterson's Theta, θ_W, and Nucleotide diversity, π, (also called θ_π). These two metrics of diversity are identical at population equilibrium and are estimates of $4N_e\mu$ (when the SFS follows a 1/q relationship), with effective population size N_e and per-generation mutation rate μ, whereas they differ in non-equilibrium demographics, under natural selection, or under other behaviors not considered in the Wright-Fisher neutral model, such as different mating systems (*43*).

First, π is described as:

$$\pi = \frac{\sum_{i=1}^{n-1} i(n-i)M_i}{n(n-1)/2},$$

and θ_W as:

$$\theta_W = \frac{\sum_{i=1}^{n-1} M_i}{\sum_{i=1}^{n-1} 1/i},$$

where $\sum_{i=1}^{n-1} 1/i$ is the *n-1*th Harmonic number, which serves to scale the segregating sites based on the assumption that the abundance of mutations follows a 1/q SFS. The diversity metrics π and θ_W are both functions of the SFS, as opposed to Fisher's α from the Species Abundance Distribution, which is a parameter that changes the shape of the distribution.

Although often nucleotide diversity π is reported as a typical measure of genetic diversity of a species, since it can be calculated for a single genome and it captures the process of inbreeding of a population (*17*), classic literature relating germplasm management for conservation and breeding has advocated for allelic richness (*44*).

II.3 Spatial genetics and the mutations-area relationship (MAR)

Since its inception, a number of concepts in population genetics have dealt with genetic variation in populations of different sizes, or populations separated in space. For instance, one

classic result in population genetics is the relationship of $\pi \approx 4N_c\mu$, which relates genetic diversity π with the effective population size N_e and the mutation rate of the species μ. A relationship which is still studied nowadays in an effort to reconcile data with theory (*17*).

In 1943, Sewall Wright turned to study the genetics of multiple populations within a species. He proposed that populations sampled further apart geographically must differ more in allele frequency due to more independent drift (*45*), leading to the commonly used correlation between geographic distance and the metric of differentiation F_{ST}. Most prominently, the use of correlation in the accumulation of mutations of populations that are geographically close or share evolutionary history has been uncovered using dimensionality reduction approaches such as PCA (*46*).

Despite these enormous advances in understanding spatial genetic structures, surprisingly little quantitative work has been done to parametrize the loss of genetic diversity by direct loss of habitat.

Because of the abundance of rare mutations in populations, it is straightforward to think that the more area and individuals sampled, the more segregating sites will be found. Analogous to the Species Area Relationship (SAR), $S=cA^z$, we should thus be able to estimate the equivalent scaling for a mutations-area relationship (MAR):

$$M=cA^z,$$

with a scaling $z = z_{MAR}$, which corresponds to the slope of best fit in a log-log-plot of A and M for a given species within its geographic range. (Other functions are often fit empirically for SAR datasets, which we explore later in section III.3. We work with the power law because of its historical use, mathematical convenience, and because other more complicated functions only improved fitting marginally, see Table S4).

This differs from other efforts to understand the number of segregating sites or heterozygosity differences across species that differ in their total census size or geographic distribution (*47*, *48*). The MAR instead is built within a species, as its ultimate aim is to relate the number of mutations left in a species as it loses spatial populations.

Below we derive what are the expectations of MAR taking two opposite scenarios of neutral population evolution, and study how many segregating sites or mutations M are discovered with increasing area in the simulations. We further test the scenario of meta-populations in space with varying migration rates and neutral or natural selection processes.

II.3.1 Panmictic population

The expected number of mutations, M, is a constant that depends on the mutation rate, μ, and the expected total branch length of the population genealogy, L, with $M=\mu L$. Under the coalescent, the total branch length is equal to the number of lineages or individuals sampled from the population, n, times the time of the genealogy during which there are such lineages, T_n, plus $n-1$ times the time in the genealogy with such number of lineages, and so forth:

$$L = nT_n + (n-1)T_{n-1} + ... + 2T_2.$$

Under the coalescent,

$$E[T_n] = \frac{2Ne}{n(n-1)},$$

and thus:

$$E[L] = n\frac{2N_e}{n(n-1)} + (n-1)\frac{2N_e}{(n-1)(n-2)} + ...,$$

which simplifies to

$$E[L] = 2N_e(\frac{1}{n-1} + \frac{1}{n-2} + ... + 1) = 2N_e H_{n-1},$$

where H_{n-1} is the (n-1)th harmonic number. This is of course related to one of the diversity metrics (section II.2), where Watterson's Θ_W scales the number of segregating sites (M) by the harmonic number of sampled individuals. This is based on the expectation that as more individuals are sampled, we expect to discover more mutations proportional to the above harmonic number. Because such number is not so easy to work with to create an expectation for z_{MAR}, we further simplify this expectation following the Taylor expansion approximation of the harmonic number:

$$H_n = \gamma + \log(n) + \frac{1}{2n} + O(\frac{1}{n^2}) \simeq \gamma + \log(n) + \frac{1}{2n},$$

which we can further approximate as:

$$E[L] \approx 2N_e \log(n-1) + c.$$

Therefore, assuming a constant mutation rate and effective population size (N_e) under panmixia, M grows following $log(n)$. In such a case, a log-log plot (typical power law plot) does not display a linear relationship, and the slope is asymptotic to $z \to 0$ for $N \to \infty$. On the other hand, with low values of x (area or individuals sampled close to 0), the slope z_{MAR} will be incorrectly high. We can show this effect trivially by studying the local derivative of the function $log_{10}(M) = log_{10}(log(N))$. The local slope of that function is an approximation of our z_{MAR} parameter. This can be locally estimated at any given point N by taking the derivative:

$$\frac{d\log_{10}(\log(N))}{d(\log_{10}(N))} = \frac{1}{\log_{10}(N)\log(10)}.$$

The implication of this nonlinear function is that if we sampled only few individuals or areas of a species (e.g., n=100), even if this species was completely panmictic we would expect a non-zero z_{MAR}, a value that will change with sampling effort. We can roughly approximate z_{MAR} by the local slope of the number in the midpoint of the graph, e.g., for n=100 we look at the slope at $n=50$, and obtain $1/(log_{10}(50) \times log(10)) \cong 0.256$. Therefore, with small sample sizes, this parameter will not be helpful to understand whether a species behaves panmictically or is limited by migration, which may be problematic for estimates of genetic diversity loss later. We can visualise our expectation of the z_{MAR} under panmixia plotting the first derivative above (Fig. S5). Because—as we will show below—we do expect a power law relationship under a migration-limited scenario, z_{MAR} should theoretically not change with sample size. The graphical study of the (non-)linearity of the log-log plots between the number of mutations and area sampled should be diagnostic to this problem (We see for

instance that *Pinus contorta* has a highly nonlinear relationship, likely due to the use of ascertained intermediate frequency markers instead of genome-wide data, Fig. S22).

Finally, we used msprime (*49*) to corroborate this finding (z_{MAR} being constant with respect to sample size) with simulations, simulating 1600 demes in a 40x40 grid of demes or populations of $N=N_e=1000$ that are completely panmictic (universal gene flow or dispersal, so this is equivalent to a single panmictic deme). We observed the z_{MAR} for $t=100...10,000$ generations in log_{10} increments. After this time, we sample $n=1...100$ individuals in increasingly large groups of adjacent demes. The range of estimates of z_{MAR} in these simulations was 0.07-0.15.

Fig. S5 indicates that the minimum average z_{MAR} even under panmixia would continuously increase with lower numbers of individuals of a species sampled. This is due to the fact that the site frequency spectrum is not fully sampled with small numbers of individuals. Therefore, we devised an approach to rescale $z_{MAR.}$

II.3.2 Scaling z_{MAR} for low sampling and low census size

Let $z_{pan\text{-}n} = E[z_{MAR} \mid n, panmixia]$, be the expected value of z_{MAR} of a panmictic species given that we only have small sampling of n. Although theoretically z_{MAR} should approach 0, with small samples it can be upwardly biased. In order to force the possible values of z_{MAR} to range 0-1 despite small sample sizes, we can scale it as:

$$z_{naive\ scaled} = (z_{MAR} - z_{pan\text{-}n}) / (1-z_{pan\text{-}n}).$$

In words, this moves the purple line in Fig. S5 to zero, stretching the space above it accordingly.

Most species have census sizes so large that z_{MAR} should indeed approach 0 under panmixia, so we should correct the sample estimate z_{MAR} to range 0-1. However, some species have such low census size N that even if we sample all individuals of a species, the sample size will still be small. In those cases, we should not scale z_{MAR} to range 0-1, but rather scale it from $z_{pan\text{-}N}$ *- 1,* where $z_{pan\text{-}N} = E[z_{MAR} \mid N, panmixia]$ is the expected value of z_{MAR} given a census size N (plants or animals living in the wild). The updated scaling approach for both census and sample size would then be:

$$z^*_{scaled} = (1-z_{pan\text{-}N})\ (z_{MAR} - z_{pan\text{-}n}) / (1-z_{pan\text{-}n}) + z_{pan\text{-}N}.$$

Note that this scaled estimate must be conservative because while we adjust the minimum z for the average value expected for low sample sizes, we do not adjust for the maximum possible z, which only under very extraordinary theoretical conditions can be z=1, namely under an unrealistic complete disconnection of populations by gene flow (see below). Because deriving the maximum z would require more biological knowledge of the species' demography, landscape connectivity, genome structure, etc., and because we rather create conservative estimates, we do not create further scaling approaches.

II.3.3 Meta-populations in space

A more realistic simulation than a panmictic population is that of the same 40x40 deme grid where migration can happen between adjacent demes. This migration rate can be changed to understand the effect of population structure and migration on z_{MAR}. Under no migration (or very low migration), we expect the mutations in two distinct populations (and thus their SFS) to be (almost) completely independent. Hence, when explored demes are doubled (N_e doubles), we discover twice as many mutations. In this case, the number of mutations should scale linearly with the area, so we expect the following to be true: $M=A$, $log(M) = log(A)$, and $z_{MAR}=1$. Our analyses under different sampling schemes, and with different numbers of "burn-in generations" (generations since a single deme colonised the full 40x40 space) confirm that z_{MAR} approaches 1 in the limit of low migration (see Table S1 and Fig. S6). Different from the panmictic situation, as we increase the sampled area, we not only increase n, which would lead to a $log(A)$ in mutations, but also increase N_e.

These simulations corroborated that we can recover z_{MAR} values ranging between 0-1 just varying migration and burn-in generation parameters. We found that it was both the time of the system to reach an equilibrium as well as the migration rate that determined z_{MAR}. In the future, it will be interesting to study different non-equilibrium scenarios to better understand how genetic drift, gene flow, and different landscape structures may shape the z_{MAR} .

II.3.4 Metapopulations in space with local adaptation

In order to simulate local adaptation, we use the individual-based simulation software SLiM (*50*) following the approach of (*51*). These simulations were set up for 196 demes arranged in a 14 x 14 grid. Each grid cell contains a population of $N=1000$ and has an environment attribute, e, which varied spatially from the lower-left to the upper-right corners (approx. $-7 < e < 7$). 12 locations in the genome were allowed to be under directional natural selection. The selection coefficient was fixed for a simulation, and grid runs were conducted with $0<s<0.05$, but this selection would vary based on the environmental selection value of a grid cell, according to $e \times s$. Therefore, these alleles are antagonistic pleiotropic. Selected mutations across the 12 loci in the genome behaved additively (e.g. if an individual in grid cell i had two of the selected mutations, fitness would be $w=1+2s \times e_i$). The migration rate varied from one individual in a billion (1×10^{-9}), to one individual every ten (1×10^{-1}). Finally, the mutation rate was set to 10^{-8} mutations/bp/generation and the recombination rate to 10^{-7} crossovers/bp/generation.

These results, together with individual-based simulations, corroborate what we had observed with coalescent simulations, i.e. that z_{MAR} is lowest with a high migration rate. The simulations also appear to show a negative effect of selection on z_{MAR} . Generating a linear model fitting migration rate and selection and their interaction to understand what factors explain the scaling coefficient: $z_{MAR} \sim log_{10}(m) + s + log_{10}(m)\ s$; we confirm that both had a significant effect, and that selection significantly reduces z_{MAR} (Fig. S7, see below summary Table S2). This may seem counterintuitive, as one may expect that locally-adaptive mutations are rare and will be localised only to where they are adaptive. More work is necessary to understand the signatures that spatially-varying natural selection (and its different types) create on z_{MAR}, but we can think that under migration limited scenarios (where z approaches 1) adaptive alleles and their linked mutations permeate faster to similar neighbour environments than neutral alleles.

II.3.5. Metapopulations in space with purifying selection

To understand the effect of purifying selection on z_{MAR} we also ran 2D simulations with a fraction of the genome allowed to be globally-deleterious (i.e. independent of the spatially-varying environment). We simulated an increasingly strong purifying selection ($|s|$ range from 0.0 to 0.1), simulating roughly that 29% of the genome of Arabidopsis is coding (arabidopsis.org) and mutations can be deleterious. We also varied the degree of recombination. Following our expectation, with stronger purifying selection deleterious mutations are pushed to lower allele frequencies, stopping their geographic spread, which increases z_{MAR}. Recombination rate appears to have a minor role on z_{MAR} (Fig. S8).

II.3.6 Continuous-space non-Wright-Fisher models

In order to confirm z_{MAR} generality in highly realistic conditions and its behavior through the population extinction process (II.4), we set up SLiM simulations in continuous space using non-Wright-Fisher dynamics (*50*). Spatial population structure in these simulations was established through individual dispersal, local mate choice and spatial competition, which we chose to lead to realistic values of F_{ST} across space. Spatial competition also acted as population control, by keeping the total population size below a target carrying capacity through direct effects on individual fitness. In addition to competition, fitness was also affected by individual age as well as by a polygenic trait under stabilising selection. A subset of variants (final proportion ~10%) directly affected this trait with effect sizes drawn from a Gaussian distribution with mean = 0.0 and standard deviation = 0.1, and a fitness penalty was incurred by deviating from the optimal trait value using a Gaussian fitness function centered at the optimum and with a standard deviation = 5.0. We initialised functional variation for SLiM using neutral coalescent simulations with msprime (*49*) to reduce the computational burden of burn-in, and loaded the resulting tree sequences into SLiM (*52*, *53*). We drew functional effect sizes for these variants, placed individuals into continuous space, and ran simulations forward-in-time for 5,000 generations. After that, the geographic distribution of the species experienced impacts as expected during global change: every generation, 0.001 of one edge of the species distribution got its carrying capacity reduced to 0. This meant that over 1,000 generations the whole species would disappear (note that this is a reasonable fraction of area reduction given the estimates of yearly deforestation and habitat change in section V). We subsequently overlayed neutral mutations on the tree sequence using msprime, and analysed genomes sampled throughout the extinction process (by tracking them in the tree sequence output) and extracted using tskit. This showed that MAR of ~0.3 is established in such realistic population dynamics as well as that z_{MAR} estimated at the beginning of the simulations predicted well the loss of (Fig. S9).

II.3.7 Connection of z_{MAR} with the isolation-by-distance pattern

Ultimately, z_{MAR} is a complex integrator of evolutionary forces acting in space (mutation, migration, drift, selection) and captures how structured the distribution of a species' mutations is. Although the isolation-by-distance pattern conceptually resembles z_{MAR}, we have found no obvious analytical expression that relates both. Note that F_{ST} is defined based on heterozygosity or π, instead of the number of segregating sites (i.e., mutations M). For instance, using Hudson's estimator (*54*) to compute F_{ST} across a set of populations we calculate $F_{ST} = 1 - (\pi_w / \pi_b)$, where π_w is the diversity or heterozygosity within a population and π_b is the same parameter calculated for the meta-population. Plotting F_{ST} of a metapopulation by the distance of the farthest demes shows the typical non-linear trend of isolation-by-distance, which shows that very close populations have similar allele frequencies whereas populations further away drift apart. A challenge of F_{ST} is that it requires

pre-defining discrete populations, which is straightforward in stepping-stone simulations but hard in real data. Comparing average F_{ST} of our 14x14 spatial demes and z_{MAR}, we see that the two parameters correlate (Fig. S10C). However, it appears that for low values of F_{ST}, z_{MAR} captures more variation across the simulations (Fig. S10). These patterns were also confirmed in continuous space simulations (not shown).

II.4 The loss of mutations (genetic diversity) in space

The aim is to predict the fraction of genetic diversity loss, x_M, from shrinking of an ecosystem by an area *a.* To define all terms, we then have a past area A_{t-1} and a present reduced area $A_t=A_{t-1}-a$, and a fraction of area extinct $x=a/A_{t-1}$

We first think of the loss of genetic diversity x_M through the basic process of losing individuals. From the population genetics's coalescent theory derivation of the number of mutations or segregating sites from individuals we got the approximation *M~log(N).* Assuming the loss of area is simply the loss of individuals (*A=N*), we can derive the fraction of genetic diversity loss as:

$$x_M = 1 - \frac{M_t}{M_{t-1}} = 1 - \frac{log(N_t)}{log(N_{t-1})} = 1 - \frac{log(N_{t-1}(1-x))}{log(N_{t-1})}$$
$$= 1 - \frac{log(N_{t-1}) + log(1-x)}{log(N_{t-1})} = -\frac{log(1-x)}{log(N_{t-1})}$$

The loss of mutations is then in the scale of: *log(1-x)*; which is very slow, as we expected from having derived the trend that under panmixia $z_{MAR} \approx 0$. A substantial loss of genetic diversity in this case only happens when population extinction is almost complete.

Species do not typically behave perfectly panmictic given different z_{MAR} values. Under population structure, we can use our relationship to project the number of mutations (genetic diversity) lost as the geographic distribution due to habitat loss or climate change following equation:

$$x_M = 1 - \frac{M_t}{M_{t-1}} = 1 - \frac{MAR(A_t)}{MAR(A_{t-1})} = 1 - \frac{A_t^z}{A_{t-1}^z} = 1 - \left(\frac{A_t}{A_{t-1}}\right)^z = 1 - (1-x)^z .$$

In the most extreme scenario of $z_{MAR} \approx 1$, the fraction loss of geographic area directly translates to the same fraction loss of genetic diversity.

Reality should be in between the panmictic and fully-migration-limited cases. With combinations of environmental selection, non-equilibrium demography, and long-range dispersal, we may get intermediate z_{MAR} values, and it will be empirical estimates that can inform us how much may be lost (Section III).

A potential caveat of this approach is that some species may partially persist in the altered habitat *a* (*55*, *56*), some genetic diversity may persist too. In such a case, we could update the MAR as the "countryside SAR", where we use habitat affinity (from section II.5, if this persistence involves first complete removal and then posterior recolonization, it can be assumed as completely lost, otherwise, the countryside MAR may be appropriate). For simplicity, we assume all habitat transformed *a* is of a single type with average habitat

affinity *h* given by global estimates of relative plant species richness in all habitats that are non-primary vegetation (*57*). This average relative richness (RR) 0.74 (sd=0.12, min-max=0.42-1.23). Using the transformation: $h=RR^{(1/z)}$ (*56*), we can rewrite our MAR as:

$$x_M = 1 - \left(\frac{A_t + ha}{A_{t-1}}\right)^z = 1 - (1 - x + hx)^z$$

If populations would not be completely lost, this will have a dampening effect in genetic diversity loss. For instance with the canonical z_{MAR} =0.3, 50% area transformed, and the above relative richness mean, the projected genetic diversity loss will be 18% for the regular MAR and 11% for the countryside MAR.

II.5 Recovery of genetic diversity after a bottleneck or local extinction

The intuition that rapid recovery of genetic diversity may be possible is likely flawed. While genetic recovery may be faster than speciation rates, which are on the order of millions of years, the time for a set of populations that went through a simulation burn-in of 1,000 generations (not yet in diversity equilibrium), and that suffer an instantaneous 5% reduction of area and an instantaneous recovery (e.g., through reforestation) would range from 20-90 generations. This number of generations for long-lived species would translate into centuries or millennia of recovery without further impacts. About 49% of simulations – including every simulation that reached equilibrium (burn-in generations >10,000) – have a recovery time of more than a thousand generations (Fig. S11).

III. The mutations-area relationship with the 1001 Arabidopsis Genomes

We begin testing the idea of a general mutations-area relationship using the extensive sampling of the model plant species *Arabidopsis thaliana* and the 1001 Arabidopsis Genomes Project (*19*). This section will serve as a case study to explore different approaches and biases when building MAR to then apply the learned lessons across species (section IV).

III.1 The Site Frequency Spectrum of the 1001 Arabidopsis Genomes

We began analyzing the frequency distribution of 11,769,920 biallelic genetic variants (i.e., mutations), which is typically called the Site Frequency Spectrum (SFS) in population genetics.

To showcase the similarities to the Species Abundance Distributions (SAD), we use the Whittaker plot of mutation rank abundance (Fig. S12, S13) that suggests a log-normal of S-shape may be the best fitting model (Table S3). For a review listing many popular models, see (*58*), and for implementation details of 13 SAD models see the thorough manual of R package SADS (*59*). As we shall see later, the log-normal distribution seems to be the best fit across species (Fig. S13, Table S3).

Although model AIC captures best the fit of a curve accounting for the difference in parameter complexity of each model and the statistical distributions behind, we often are interested in the variance explained. We then calculated a proxy of predictive accuracy using a pseudo-R^2 approach of the difference between the model fit and the observed data as: $R^2 = 1 - \frac{SS_{res}}{SS_{tot}}$. For *A. thaliana*, we used 10,000 SNPs sampled at random to an accuracy of

over R^2 >0.999 for both the top log-Normal model and the bottom log-Series model, indicating that all "commonness of rarity" models must have a pretty good fit of mutation frequency data.

The typical SFS from population genetics is of course not implemented in current packages for Species Abundance Distributions like R sads. For comparison, in the main text we also calculate the log likelihood and AIC of this following the standard population genetics likelihood:

$$logL = \sum_i log(\frac{1}{Nq_i}) - log(H_n(N-1))$$

,

where N represents the number of individuals in a sample, and q_i is the minor allele frequency of a SNP in the sample, in the main text calculated for i=1…10000 random SNPs (see main text). As before, H_n is the harmonic number function.

III.2 Building the mutations-area relationship (MAR)

In the following, we explain how the area was estimated that was used to compute z_{MAR} on real world data. In short, we used a grid on the world map, with samples placed on the map based on their geo-coordinates of origin (Fig. 1 in main text). We first create square spatial subsamples of the *Arabidopsis thaliana* geographic distribution (Fig. 1, Fig. S15) and quantify diversity M as the total segregating sites. Excluding zeros, these two variables are fed to the sars_power() function from the R SARS package (*60*).

Although the power law mutations-area relationship was already theoretically motivated (II.3), here we also fit different types of functions typically applied to the Species-Area Relationship. Doing this, we reach the conclusion that multiple models perform very similarly, and the classic power law is among the top models, see Table S4. Although small marginal fitting accuracy could be achieved with other models, for mathematical convenience and historical continuity, we use the power law for later sections and the study of MAR across species (Sections IV and V).

Because in the species literature it is recommended to only quantify richness of endemic species (*61*), we also count segregating sites that are private to the area subsample, creating the equivalent endemic-mutations-area relationship (EMAR) (*61*). The MAR slope and 95% Confidence Interval was z = 0.324 (0.238 - 0.41) (Table S5, Fig. S14 A), while the EMAR was z = 1.241 (1.208 - 1.274) (Table S6, Fig. S14 B). Interestingly, the endemics-area relationship of $z \approx 1$ resembles that of endemic species, whereas the total mutation relationship with area is above that of species relationships, which typically follows the canonical $z \approx 0.2 - 0.4$.

We must note that EMAR, the genetic analogy of the Endemic-(species)-Area Relationship (EAR) may not be that meaningful when analyzing genomic data (we did not find a way to theoretically motivate it in section II), and later we see it overestimates loss in our simulations (Fig. S18)

III.3 Testing for potential numerical artefacts

We wondered whether MAR estimates may be affected by some numerical artefacts in our software pipeline (available at https://github.com/moiexpositoalonsolab/mar). For instance, real world data may have uneven sampling in space, the spatial resolution of georeferenced samples may vary, projection of samples into gridded maps may have limited resolution, software pipelines may produce biased estimates, etc. To test this, we conducted several experiments:

Lower bound of the method for z_{MAR}. Our first experiment when building the MAR aimed to make sure that spatial sampling, or some unknown bias in genome sequencing, or the number of samples used, are not creating artificially large $z_{MAR.}$ We then simulated a mock dataset of *A. thaliana* with the same number of mutations, samples, and using the original geographic locations. The number of SNPs were also sampled in a way that we created a canonical 1/q SFS for the whole species. Under no biases, we then expect the MAR to follow the theoretical derivation under panmixia with a z~0. This exercise confirmed we get a value approaching zero: z=0.033, (-0.095 - 0.162).

Grid sizes, area calculations, and non-random spatial sampling. In order to streamline geospatial operations, we implemented the MAR relationship calculations in this project using R raster objects (*62*). This required projecting the collected samples of a species and the observations of any given mutation into a world map (i.e., each mutation's geographic distribution). Necessarily, in order to be able to assign areas to sets of samples or mutations on the map, the projection requires the choice of a grid size. The larger the grid size (e.g., lower spatial resolution), the faster the spatial operations can be performed. Further, for larger grid sizes, we expect the slope of MAR to be more influenced by larger-scale patterns, while for smaller grid sizes, the MAR will be influenced by smaller-scale patterns. To test this, we repeated the subsampling of *A. thaliana* distribution with grid sizes ranging 0.1 degrees latitude/longitude (roughly 10km side-length in temperate regions) to 10 degrees (roughly 1,000 km side-length). The estimates were roughly consistent between 0.4-0.6, but increases in value at larger grid sizes (row in Table S7 for large grid size values), a scale-dependent pattern that resembles results of SAR of species in ecosystems fitted at different scales (*15*).

Because we often have sparse samples of individuals in space, we devised two strategies to calculate areas during the subsampling of MAR (see cartoon in Fig. S15): (A) the total square area of the minimum and maximum latitude/longitude values of all the samples analyzed. That is, simply the area of the red box in the figure. (B) the sum of areas of grid cells that contain at least one sample. That is, the sum of the grey squares within the red box in the figure. In addition, we also calculated the MAR relationship assuming the total area is equal to the number of individuals (A=N) (which should be theoretically equivalent to a grid of very high resolution where we end up with a maximum of one individual sampled at any grid cell).

Table S7 values suggest there is a dependency of z_{MAR} with the grid size when areas are calculated as the sum of grid cells with at least one sample. Our intuition for this pattern is that lower resolution grids (e.g., 5 degrees side) lead to some grid cells having many samples, which would increase the number of mutations discovered when discovering the area. On the other hand, the calculation of z_{MAR} using the total area does not seem to affect the z_{MAR} estimate; however, because large areas often do not have samples (limiting the potential to find new mutations), it creates a higher variance in the estimate of z_{MAR} (see confidence intervals in Table S7 and Fig. S16). Here, we favored consistency of z at the expense of

broader, more conservative confidence intervals. All the estimates reported below and in the main text therefore use the total area approach.

Geographic subsampling strategy (inwards, outwards, random). It has been indicated that the way the Species-Area Relationship (SAR) and Endemics-Area Relationship (EAR) are created may create differences in the scaling parameter *z*. The plots and estimates above were produced by randomly placing boxes of different size or area across the distribution of the species. Often, however, either discovery of species or extinction happen in certain patterns. For instance, we often imagine sampling an ecosystem concentrically outwards from a focal point, whereas we may think of the extinction process of species area reductions being concentrically inwards (*61*). Because these patterns seem of importance, we also calculated the MAR and EMAR outwards from the latitude and longitude median of all the samples in the map, moving outwardly until the map is filled (Fig. S17, Table S8). Likewise, the inward pattern is conducted in an inverse manner.

Incomplete sampling of the species. To check whether the relationship holds with few individuals of a species or limited geographic distributions, we compared the species-wide MAR with that of subset populations. Downsampling the native distribution of *A. thaliana* to a region within North-East Spain (-2.00–4.25 degrees East, 36.52–42.97 degrees North), or to a region within Germany (2.69–13.73 degrees East, 50.0–52.0 degrees North), and using only 1,000 SNPs, we recovered z_{MAR}= 0.423(0.233-0.614) for Spain and 0.525(0.242-0.807) for Germany, which were close to the estimate based on the whole distribution (Table 1). This result is reassuring in that if migratory patterns are relatively homogeneous, one may be able to estimate this parameter from a subset of the species distribution. For heterogeneous population structure cases, we expect incomplete sampling to produce unreliable estimates.

Number of genome-wide SNPs used. To check whether different numbers of SNPs used for the analyses would lead to different z_{MAR}, we conducted analyses with random subsets consisting of 100, 1,000, and 10,000 SNPs, replicated 3 times. Estimates had a coefficient of variation of 4.7%, which is way below the standard error of typical estimates (Table 1).

Locally-adaptive variants. We then aimed to understand the effect of utilizing SNPs that appear to be related to adaptation. To study this, we utilized an outdoor climate-manipulated experiment that recorded fitness data (survivorship and reproduction output of seeds) for 515 *Arabidopsis thaliana* ecotypes part of the 1001 Genomes set in 8 environments (Exposito-Alonso, 2019). We devised two sets of alleles: 10,000 that were negatively correlated with fitness in a Genome-Wide Association across 8 different environments, and 10,000 alleles that were associated positively with fitness in one environment but negatively in another (antagonistic pleiotropic). The MAR relationship was computed as before and compared to the original random (putatively neutral) set of alleles from the previous sections (Table S9). Although we see a trend that locally-adaptive alleles have a slightly higher *z*, estimates overlap. The effects seen here of having smaller *z* for adaptive alleles than neutral variation could, however, be due to top GWA SNPs often being ascertained to higher frequency than background SNPS.

III.4 Local population extinction in Arabidopsis

Using the MAR framework, we can make projections of loss of mutations (or its inverse, the remaining genetic diversity. By doing this, the known intuition is that with $z > 1$ (as from EMAR) the decrease of diversity is much faster than the decrease of habitat, but with $z < 1$ (as from MAR), there is a (desirable) slower dynamics of genetic loss. In the latter, despite habitats disappearing, reservoirs of mutations distributed across different locations enable conservation of certain variation. To study which one is more likely and to observe the stochastic nature of genetic diversity loss, we simulated in silico population extinctions of map cells from the Arabidopsis map (Fig. 1) and directly estimated from the genome matrix of remaining individuals the remaining genetic diversity. These simulations were implemented to capture different hypothesised patterns of extinction (see main text). All, however, agree with the more hopeful estimate of $z_{MAR} \approx 0.3$.

To study the fit of the genetic loss predictions based on MAR relationships and the results from computer simulations, we calculated a pseudo-R^2 based on the squared differences between the predicted line and the "observed" genetic loss as: $R^2 = 1 - \frac{SS_{res}}{SS_{tot}}$. This results in a high fit R^2=0.872 of the MAR, built from random samples of distribution areas, while the EMAR had a poor fit due to overestimation of genetic loss: R^2=-0.710 (negative values indicate predictions are worse than the mean of the data).

III.5 Potential impacts of genetic loss in adaptability

Although likely imperfect, Genome-Wide Associations could help to understand the relevance of mutations in different frequency classes in model organisms such as *Arabidopsis thaliana*. Fig. S19 shows the site frequency spectrum and a metric of the "total accumulated effect in fitness" of the alleles in every bin. Effect sizes were retrieved from GWA on lifetime fitness of 515 ecotypes in outdoor experiments (*29*). The average effect size across 8 fitness GWA from 8 experimental combinations were used: high/low precipitation, high/low latitude of outdoor stations, and high/low plant density. This exercise showcases the phenomenon that low frequency variants often have strong effect sizes, which is expected under a stabilising selection quantitative model (*63*). Because low frequency alleles will be the first to be lost during a bottleneck (as would happen with the rapid extinction of populations of a species), we may expect to lose variants that are related to fitness and thus potentially lose diversity that could be advantageous in some environments. Alternatively, deleterious mutations are also expected to be at low frequency, in which case would also make them more easily lost.

To further build intuition on the progress of extinction in relation to loss of genetic diversity that is not neutral, we repeated warm edge extinction simulations with several subsets of alleles (Fig. S20): randomly selected SNPs, SNPs that were associated positively in 2 environments (low precipitation Spain and high precipitation Germany) (labelled globally positive), and SNPs that were associated positively in one environment and negatively in the other (labelled antagonistic pleiotropic or putatively locally-adaptive). This supports our intuition that although putatively functional alleles (or alleles tightly linked to such functional ones) may have slower loss dynamics than neutral variants due to a high frequency and z_{MAR}, certain population extinction patterns may actually lead to rapid loss of potentially-adaptive genetic diversity (Fig. S20). The complexity of these patterns, together with the evolutionary feedback created by lowering genetic standing variation that affects

fitness, make the inference of adaptive capacity loss even more difficult than just inferring the loss of genetic diversity itself.

Finally, we also retrieved allele effects of different traits (fitness under drought or well-watered conditions, plant size, plant growth rate, seed dormancy, flowering time, and water use efficiency [wue], data available at: https://aragwas.1001genomes.org, https://arapheno.1001genomes.org/). For each trait, we extracted the 10,000 SNPs with the lowest *P*-value and their effects a_i. We then computed two proxies of adaptability based on these i=1…10,000 variants. The additive genetic variance: $Va = \sum_i p_i(1-p_i)a_i^2$; which also accounts for the frequency of variants p_i, as variants of intermediate frequency contribute more to the population trait variance than rare variants. And a simpler metric that just sums the cumulative summed effects of variants, $\sum_i a^2_i$. We then visualized these proxies of adaptability that each trait could confer in a population whose trait is under selection, and how this is eroded in warm edge extinctions (Fig. S21).

III.6 Case study of a massive natural bottleneck

A recent colonisation of North America by *Arabidopsis thaliana* can help us understand the recovery of genetic variation. Whole-genome sequencing of 100 specimens of North American *A. thaliana* indicates that it migrated from its native range of Europe to North America in the 17th century, and began spreading across the continent from a genetically-homogeneous population (*64*). Despite ideal conditions to re-gain genetic diversity—a continental population expansion aided by human travel (*65*, *66*)—only ~8,000 new mutations were detected through spontaneous accumulation, equivalent to only ~0.067% of the species-wide native genetic diversity. Because most of these mutations are at very low frequency, as expected during population expansion, the scaling of genetic diversity with area is approximately 1 (z_{MAR} = 1.025 [CI95%: 0.878 - 1.173]).

IV. The mutations-area relationship in diverse species

Every dataset was retrieved online either from the published article in the form of VCF or fastq files, or provided by the study authors upon request. All datasets were first transformed into PLINK files using PLINK v1.9 (*67*). For computational efficiency, and since we showed random subsampling does not appear to affect calculations of z_{MAR} (Section III.3), we conducted all analyses with up to 10,000 randomly selected SNPs for each species sampled genome-wide, or in the largest chromosome for those species with large genomes. We aim to use mostly unfiltered SNP datasets to avoid ascertainment biased toward intermediate frequency SNPs, and therefore we did not apply a MAF filter for any analyses. By default, PLINK transforms SNP matrices into biallelic (if multiallelic, it takes the two most common alleles). Although the preservation of structural genetic variation may also be relevant and may have important consequences in adaptation (*68*), we do not expect dramatic differences in their scaling relationship compared to biallelic SNPs, as their SFS are relatively similar (Structural variants may show a skew to lower frequency, resulting in steeper z_{MAR}. By excluding those, our analyses may be conservative). In order to properly characterise the geographic distribution of a mutation using all available geo-tagged individuals, we filtered for genotyping rate (plink --geno), and the final value is reported per dataset.

Details for dataset processing or homogenization are described below.

- The 1001 Arabidopsis Genomes Consortium (*19*) generated a WGS Illumina sequencing dataset of *Arabidopsis thaliana* comprising 1,135 individuals and 11,769,920 SNPs. The VCF with the data is available at: https://1001genomes.org. The raw sequencing data is available at https://www.ncbi.nlm.nih.gov/bioproject/PRJNA273563. These included recently colonised regions such as North America or Japan. Analyses of z_{MAR} were calculated only for the native range, which comprises most of the species diversity (>99%) and 1001 individuals. For computational efficiency, we conducted analyses using randomly sampled SNPs from chromosome 1, as we did not observe any difference when sampling from other chromosomes. A number of MAR approaches were tested in this species (section III). For homogeneity, the final reported estimate (Table 1) was conducted following the same procedures as other species with a random sample of 10,000 SNPs.

- Lucek & Willi (*69*) recently published a dataset of WGS Illumina sequencing 108 *Arabidopsis lyrata* individuals from North America, which the authors directly shared as a VCF. The raw data is available at https://www.ncbi.nlm.nih.gov/bioproject/?term=PRJEB30473. We retrieved the latitude/longitude data from the supplemental material. We applied a genotyping rate filter ending with a dataset of 0.955431 genotyping rate. 10,000 SNPs were subsetted at random from the genome-wide data.

- Kreiner et al. (*70*) WGS Illumina sequenced 165 individuals of *Amaranthus tuberculatus*. The raw data is available in the link https://www.ebi.ac.uk/ena/browser/view/PRJEB31711. The authors provided a VCF. Overall, 155 individuals contained latitude and longitude information and were kept for the analyses. The genotyping rate was 0.98162 and we subsetted randomly 10,000 SNPs.

- Supple et al. (*71*) generated a dataset of *Eucalyptus melliodora* of 275 individuals from 36 broadly distributed populations. The dataset was produced by Illumina sequence Genotyping-by-Sequencing (GBS) libraries digested with ApeKI as in Elshire et al. (2011). The raw data is available at https://www.ncbi.nlm.nih.gov/bioproject/PRJNA413429/. The authors provided the dataset in PLINK format. Genotyping rate was 0.769807 but we did not apply a further filter to avoid reducing the total number of variants. We conducted analyses with all 9378 SNPs. The genotyping rate in this dataset is likely not problematic as the total number of GPS locations is 36, with multiple individuals sampled closely. This sampling scheme probably allows to characterise an allele's distribution correctly despite the lower genotyping rate.

- Vallejo-Marin et al. (*72*) generated a GBS dataset of 521 Mimulus plants, with 286 samples being *Mimulus guttatus* from its native distribution. Libraries for Genotyping-By-Sequencing were prepared with PstI enzyme as described in Twyford & Friedman (2015) and sequenced using Illumina. The VCF of this dataset is available at http://hdl.handle.net/11667/168 and was also directly shared by the authors. After applying a filtering for missingness, we ended up with a genotyping rate of 0.904192 and 1,498 SNPs, which were used for the analyses.

- Lovell & MacQueen (*73*) generated a WGS Illumina sequencing dataset of Switchgrass, *Panicum virgatum*, of a collection of 732 individuals and 33,905,044 variants. The raw data is available at: https://www.ncbi.nlm.nih.gov/bioproject/PRJNA622568. The authors provided a VCF file and latitude/longitude tables. 576 individuals were from natural collections. The dataset contains also other collections such as cultivars, which were not used to build the MAR. The genotyping rate was 0.976393 and analyses were conducted with 10,000 SNPs drawn from the largest chromosome.

- MacLachlan et al. (*74*) generated a SNP chip dataset of *Pinus contorta* comprising 929 trees with latitude and longitude information and 32,449 SNPs. Genotyping was conducted with the AdapTree lodgepole pine Affymetrix Axiom 50,298 SNP array and data was provided in the supplemental material of the paper along with custom scripts to parse the data. The database is available at https://datadryad.org/stash/dataset/doi:10.5061/dryad.ncjsxkstp. The genome matrix was transformed into PLINK. The genotyping rate was 0.959146, and analyses were conducted with 10,000 randomly drawn SNPs. The fact that this dataset was created with ascertained SNPs likely generates a frequency bias. In Fig. S22, one can see that this may be a problem to calculate z_{MAR}, as the mutations~area graph appears nonlinear and rapidly saturates. This confirms the expectation that SNPs are ascertained to be common, as they are discovered immediately with very few samples.

- Tuskan et al. (*75*) WGS Illumina sequenced 882 *Populus trichocarpa* trees. The dataset includes 28,342,826 SNPs. The data is available under this DOI https://doi.ccs.ornl.gov/ui/doi/55 which redirects to a globus data sharing platform. The authors provided the dataset as a VCF along with latitude/longitude coordinates. This dataset was downsampled to the first chromosome. The genotyping rate was 0.921191, and 10,000 SNPs were randomly sampled for analyses.

- The Anopheles gambiae 1000 Genomes Consortium (*76*) (Phase 2) produced Whole-Genome Illumina sequencing data for 1142 wild-caught mosquitoes of *Anopheles gambiae*. All raw and processed data are available through https://www.malariagen.net/data. We downloaded a VCF and latitude/longitude coordinate files. The VCF was filtered for genotyping rate ending up at a 0.998895 rate. For efficiency, 10,000 randomly-selected SNPs from the VCF of the largest chromosome 2L were used for analyses downstream.

- Fuller et al. (*77*) WGS Illumina sequenced 253 coral individuals of *Acropora millepora* in 12 reefs. The dataset was downloaded as fastq files from the published online material from https://www.ncbi.nlm.nih.gov/bioproject/?term=PRJNA593014, and SNPs were called as described in the supplemental material ending with 17,931,448, which were filtered to achieve a genotyping rate of 0.935709 for a total of 2,512 SNPs, which were used in the analyses.

- Ruegg et al. (*78*) generated a dataset of 219 birds *Empidonax traillii*, for which 199 could be matched with geographic coordinates. SNPs were ascertained from several publications using RAD seq and Fluidigm 96.96 IFC described and available in their repository https://github.com/eriqande/ruegg-et-al-wifl-genoscape. A total of 349,014 SNPs were parsed using their custom scripts and we transformed them into PLINK files. A genotyping rate filter was applied ending with a 0.96061 rate and 195,700 SNPs. 10,000 SNPs were selected at random for downstream analyses. Similarly, as with the *Pinus contorta*, the incorporation of some ascertained SNPs in the dataset based on Fluidigm technology could lead to quick saturation of the MAR curve (Fig. S22).

- Bay et al. (*79*) generated a dataset of 199 *Setophaga petechia* birds using a Restriction site–associated DNA sequencing (RAD-Seq). The raw data is available at https://www.ncbi.nlm.nih.gov/bioproject/421926. The authors shared a VCF file, with a genotyping rate of 0.962419 and a total of 104,711 SNPs. 10,000 SNPs were selected at random for downstream analyses.

- Kingsley et al. (*80*) produced a dataset of 80 *Peromyscus maniculatus* deermice, for which 78 could be matched with geographic locations. The SNP dataset was produced using MY-select capture followed by Illumina sequencing. The VCF and PLINK files are available via Figshare at https://doi.org/10.6084/m9.figshare.1541235. The dataset included a total of 14,076 variants which were filtered to achieve a genotyping rate of 0.940411 for 2,946 SNPs, which were used in subsequent analyses.

- We identified two published datasets for wolves. Smeds et al. (*81*) produced a WGS Illumina sequencing dataset and combined it with pre-existing datasets for a total of 349 local dog breeds and wolves, of which 230 were *Canis lupus* from natural populations. However, these samples did not have GPS locations assigned. The second dataset we identified was from Schweizer et al. (*82*), which contained 107 geo-tagged grey wolves from North America using a capture and resequencing approach for 1040 genes. The raw data is available at https://trace.ncbi.nlm.nih.gov/Traces/sra/?study=SRP065570, and meta-data along with a VCF area available at https://doi.org/10.1111/mec.13467. This data contained 13,092 SNPs at 0.993061 calling rate, and a better geographic resolution. We report data for the second dataset.

- The 1000 Genome Consortium (*83*) created WGS Illumina sequencing for over 2,504 humans and 24 unique geographic locations. We downloaded chromosome 1 from http://ftp.1000genomes.ebi.ac.uk/vol1/ftp/datacollections/1000G2504highcoverage/working/20190425NYGCGATK/ and gathered the population locations from https://www.internationalgenome.org/data-portal/population. To conduct analyses, we subsampled 10,000 SNPs at genotping rate 0.991069.

- Palacio-Mejia (*84*) used WGS for 591 *Panicum hallii* individuals to sequence at low coverage. The raw data is available at https://www.ncbi.nlm.nih.gov/bioproject/PRJNA390994. The authors shared an unfiltered VCF of 45,589 SNPs. Because of the low-coverage, stringent filters of calling rates as used for other species would lead to removing all SNPs, and we settled on a genotyping rate of 0.825824 for 242 variants, all of which were used for downstream analyses.

- Royer et al. (*85*) produced a SNP dataset using RAD-Seq based Genotyping-By-Sequencing of 290 *Yucca brevifolia* (Joshua Tree) individuals. A total of 10,695 SNPs with a genotyping rate of 0.897501 wre used for the analyses. The data was available at Dryad https://datadryad.org/stash/dataset/doi%253A10.5061%252Fdryad.7pj4t.

- Kapun et al. (*86*) produced a WGS dataset of pooled *Drosophila melanogaster*, sequencing ~80 pooled individuals from each of 271 populations as part of the European "Drosophila Evolution over Space and Time" (DEST) project. A total of 5,019 shared SNPs with a genotyping rate of 0.937697 were used for analyses. The dataset, both raw and processed, is available through https://dest.bio.

- Di Santo et al. (*87*) studied the highly-threatened species *Pinus torreyana*. They used Genotyping-by-Sequencing of 242 individuals of the last remaining populations. The dataset is available at NCBI: https://www.ncbi.nlm.nih.gov/bioproject/PRJNA840943; and the authors additionally shared a VCF. From a total set of 166,564 SNPs with a genotyping rate of 0.964632, 10,000 were randomly selected for our analyses.

- von Seth et al. (*88*) studied the highly-threatened species *Dicerorhinus sumatrensis*. They used Illumina WGS of 16 individuals of the last remaining populations. The raw data is available at https://www.ebi.ac.uk/ena/browser/view/PRJEB35511. The authors shared a VCF. In total, this comprises a set of 8,870,513 SNPs, with a genotyping rate of 0.854862, which we did not further filter due to the small number of individuals. For computational efficiency we selected 10,000 SNPs from the largest chromosome.

Information and results per species are gathered in Table 1 and its extended version, Table S10, and the average z_{MAR} across species are provided in Table S11.

IV.1 Exclusion of species from global averages

To avoid contaminating across-species averages of z_{MAR} with estimates of species whose data we do not fully trust, we conducted global averages excluding species for which we are not confident z_{MAR} reflects the correct species diversity-area relationships.

Pinus contorta showed a lower z_{MAR} than what is expected in a theoretical baseline from individual sampling (section II). This is most likely due to this being the only species for which SNPs were previously ascertained to be intermediate frequency (i.e. the genome technology was a SNP chip). This alters SFS, so we are not confident the z_{MAR} is the true parameter of the species.

Yucca brevifolia was a dense sampling of several local populations within a constrained area that is a hybrid zone. Since this species was not sampled range-wide we do not feel confident to include it in downstream analyses. The species also has a lower z than expected (Fig. S5)

Pinus torreyana only has two wild populations left, and therefore the MAR is based on two area sizes (Fig. S22). Because this is such a threatened species with already most of its range loss, we do not have confidence in the z parameter.

Dicerorhinus sumatrensis has only ~30 estimated adult individuals in the wild. Again we do not have confidence in the z parameter in such extinction-edge cases.

Homo sapiens. We exclude our own species.

IV.2 Differences across species in MAR

Although we could not see any obvious patterns relating z_{MAR} with certain groups of species (Table 1), we wondered whether any life history trait of the species analysed could explain the variation we observed (see Table S12 of traits). An ANOVA did not show any significant relationship. Because we know theoretically this parameter must be related to the degree of dispersal ability of genotypes of a species relative to the whole species geographic range, we expect traits involved in determining these to be good predictors. Future work will be necessary to validate this, as the sample size (n=19) may not permit enough power to detect these expected patterns.

While no association between life history and z_{MAR} was found (Table S13), this may be due to limited power, as the sample size of species analysed here is still small, n=20. Further studies expanding the numbers of species will be necessary to confirm or reject this expected association.

V. An estimate of global genetic diversity loss

Using the approach described in section II.4, we generated a number of estimates either per ecosystem or per species. All estimates below tried to be conservative, and thus we always used the scaled z_{MAR} values (section II.3.2.)

V.1 Estimates of ecosystem area losses

Millenium Ecosystem Assessment

Ecosystem transformation has been tracked over decades. We extracted ecosystem transformations from the Millennium Ecosystem Assessment (*22*), which estimated ecosystem transformations from presumably native systems to cultivated or urban areas by GLC2000 land cover dataset (Table S14). The forest/woodland is calculated as percentage change between potential vegetation from WWF ecoregions to the current actual forest/woodland areas from GLC2000. These provide bulk ecosystem reductions, not for a given species, but may be a good proxy for an average across species.

Intergovernmental Science-Policy Platform on Biodiversity and Ecosystem Servies

The Intergovernmental Science-Policy Platform on Biodiversity and Ecosystem Services (IPBES) recently used a PBL satellite product from the Netherlands Environmental Assessment Agency (https://www.pbl.nl/en/nature-and-biodiversity) to study the % of area ecosystem transformation in the world (Table S15). This provides an updated estimate to the Millennium Assessment as well as projections under several Shared Socioeconomic Pathways (1-3) for 2050. These were reported per region as of 2010, and for projections to 2050 (scenario SSP2). Instead of direct area, the metric is a composite of land use information to predict Mean Species Abundance (MSA), a measure of the size of populations of wild organisms as a percentage of their inferred abundance in their natural state (% MSA).

Land Use Harmonization

A global transformation metric can also be captured by the most updated land use transformation data, the Land Use Harmonization 2 (release v2e for 2015-2011 and release v2h for baseline 1850-2015) (*23*). Baseline transformation of primary ecosystems was calculated subtracting the total area covered by primary forest (primf) and primary non-forest (primn) variables between year 1850 layer (rough baseline before large-scale post-industrial impacts) and the present, 2015, as $1\text{-}A_{2015} / A_{1850}$ (Table S16).

Analyses that use projections to mid-21st century were conducted following (*89*), summing over all transitions from primary forest (primf), primary non-forest (primn), secondary forest (secdf) and secondary non-forest (secdn) lands to any other category for all years within the 2015-2050 period (see Table S10).

Global Forest Watch

We searched for timely estimates of forest reduction (based on vegetation cover) reported in the Global Forest Watch website: globalforestwatch.org/dashboards/global/ (accessed June

2021). From 2002 to 2020, there has been a global tree cover loss of 10%, with an annual tree cover loss of 0.6-1.1%.

IUCN Red List

We utilized https://www.iucnredlist.org to conduct separate searches of "plants", "amphibians", "birds", "mammals", and downloaded all records (n=82,801) with all their descriptions of classifications and threats using the download results tool. Table 17 shows a summary of all species. We separated species numbers by the guidelines IUCN Red List v15 (*24*). Several criteria are used to classify species into different categories (e.g. vulnerable, endangered, etc.). Criteria A1, A2-4, C1 all have quantitative thresholds of % of population reduction. IUCN defines population as all individuals across the range, and all subpopulations (individuals grouped geographically) need to be assessed in the population reduction criteria. Of the area criteria, A2-4 are the most common (Table S17), and most include evidence based on evidence of extent or area of occurrence (subcriteria "c"), and hence can provide rough estimates of area reduction. Therefore, we use the thresholds necessary to meet A2-4 summarized in Table S17 and in Fig. 3 in main text. Note: Near Threatened (NT) do not have a specific criteria, but species are granted this classification when they do not qualify for Vulnerable (VU) and at the same time cannot be classified as Least Concern (LC) or Data Deficient (DD). The only percentage of area reduction provided by IUCN for this category is 20-25% loss (see details in (*24*)).

Map Of Life

Current projection trends are available in the Map Of Life tools for mammals, birds, and amphibians (mol.org, see example https://mol.org/species/habitat-trend/Dicerorhinus_sumatrensis) and summarized in (*25*). We used the habitat trends as 1- A_{2017} / A_{2015} in Fig. 3, which show ranges from 0 to 100%, with an average of 5.9%.

V.2 A global estimate of genetic loss

Taking the estimates and standard error of z_{MAR} across species, and the world's reduction of ecosystems we can calculate the fraction of genetic diversity reduction following the MAR equation (section II.4), giving a range of estimates (Table S18).

Assuming the average z_{MAR}, and utilising tree cover from the Global Forest Watch (https://www.globalforestwatch.org), which estimates 0.6-1.1% of transformation per year across Canada, United States and Australia, we extrapolated genetic diversity loss in the next 50 years for tree species to be 8-15% genetic diversity loss.

Assuming that the calculated z_{MAR} estimates (Table 1) are representative of plant species, we conducted an experiment to create a distribution of % of genetic diversity loss in threatened species. We used the number of species in each IUCN category (Table S17) for a total of 54,127 plant species. For plant species, one of the evaluation criteria of percentage of population loss likely translates faithfully to area reduction in the species. Thus, the proportion of species per category gives a discrete probability distribution of the ranges of percentage of area loss: P(0-29%)=0.596, P(30-49%)=0.156, P(50-79%)=0.159, P(80-99%)=0.086, P(99%-100%)=0.003. Using a simulation-based sampling approach, we

drew 350,000 random area reductions A_t / A_{t-1} from the previous distribution and a z_{MAR} from the mean and variance of our estimates from Table 1 for plants. These were plugged into the MAR equation (Section II.4) to calculate the percentage of genetic diversity loss of these 350,000 random draws. The resulting distribution had a median and interquartile range of 17.53 % [7.51- 31.82]..

Using the Land Use Harmonization 2 dataset, we also create per-species predictions based on the % transformation of each of the sampled regions per species (Table S14). As before, the land use transformations that merit be considered area losses are all transitions from primary forest (primf), primary non-forest (primn), secondary forest (secdf) and secondary non-forest (secdn) lands to any other category. Taking all the locations where each species has been sampled, we extracted the predicted % of land use change per cell and summed over all cells where individuals had been sampled (we call this LUH^2 change '50, see column in Table S10). We also produced the alternative area loss estimate taking that at least 10% predicted habitat transformation for a grid cell renders the entire area of that grid cell as impacted or lost (we call this LUH^2 >10% change '50). These per-species area losses, in combination with the matched z_{MAR}, provided a range of potential loss estimates to 2050 ranging 0-36% depending on the species (Table S10).

V.3 Community ecology simulations and MAR

To test whether intermediate levels of MAR would be expected across species in entire ecosystems, we conducted community assembly simulations of ~100-500 species following the Neutral Theory of Biodiversity (*34*, *68*) and coalescent simulations (*49*) using the software MESS (*90*). These simulations are computationally demanding and could not run in a complete 2D spatial grid. Instead, they were simulated in a mainland-island system, with islands of increasing areas. The community forms by species colonising an empty island according to Hubbell's Unified Neutral Theory of Biodiversity and Biogeography (UNTB), where all species are equally likely to colonise and persist in the local community. Continued colonisation and migration to the local community continues to bring in new species that may or may not survive, while also continuously bringing in individuals of species already in the local community. The community assembly process ends when the community has reached an equilibrium denoted as the balance between local extinction and new species dispersing into the area (Hubbell 2001). Once the forward-time process has ended, we simulate the coalescent history of each species backward in time. For this, MESS considers the population size, divergence time, and migration rates of the meta and local communities. These coalescent simulations provide us with genetic data and ultimately diversity estimates for each species in the community.

We simulated 100 MESS communities, and for each community the size of the local community was varied from 1K to 100K. We varied the size of communities to emulate variation in area occupied by a given community because we assume as the number of individuals in a community increases from 1,000 to 100,000, so does the area occupied. All other parameters were kept consistent across each of these community simulations, and most remained at their default value. The parameters changed were the length of the sequences simulated for the coalescent-based simulations, which was fixed at 10,000 bp, and the migration rate, which was fixed at 0.01.

The simulation output was used to then compute a single z_{SAR} for the system as $S=cA^{zSAR}$, and one z_{MAR} for each species in the same way, $M=cA^{zMAR}$. This resulted in the distribution of z_{MAR} from Fig. S24. This confirmed that we can recover typical z_{SAR} and z_{MAR} values from completely stochastic neutral yet spatially structured systems such as species in communities and mutations in populations of a species.

V.4 The nested species extinction and genetic diversity loss processes

Finally, we worried that our estimates of V.2 would be mistaken as overestimates. In fact, we believe these may be underestimated. Recent policy proposals for the United Nations' Sustainability Goals emphasize that the target of protecting 90% of species genetic diversity for all species cannot leave the already-extinct species behind (*10*) (That is, one cannot protect 90% of species and leave 10% to become extinct to meet this goal). This clearly exemplifies a problem in conservation biology that what researchers can study is (most of the time) what has escaped extinction, and therefore if we do not account for extinct species in our overall estimates of genetic diversity loss we may naively think ecosystems have not suffered genetic diversity loss (i.e. in the extreme scenario, an ecosystem that has lost all but one abundant species may not really appear genetically eroded if such species is in good shape).

We then created spatial simulations in R where 1,000 species are distributed in 100x100 grid cells following a UNTB abundance distribution and then proceeded with an edge extinction of the ecosystem (see Fig. S25 for a cartoon).

Two extreme types of distributions of species can be imagined: species are randomly placed in space, or species are found mostly in perfectly contiguous ranges (We ended up using as an example a simulation with 85% of the individuals of a species found in a core square continuous distribution and 15% found outside that core in fragmented observations, as this scenario produced the canonical SAR of z~0.3). Spatial structure interestingly creates two extreme distributions of area reductions across species (Fig. S26): random placement of cell habitats essentially show that the average area reduction per ecosystem is followed by most species, while autocorrelated placement of cell habitats create a U distribution in area reductions, where at the beginning of the extinction process most species have not experienced any impact (Fig. S26B left) but at the end of ecosystem reduction virtually all species are already extinct (Note we may be at the beginning of S26B process given the data from IUCN, Fig 3C).

To study the consequence of the above differential area loss and the effect of some species going extinct on the total ecosystem genetic diversity, we conducted the next analysis: For extant species, we assumed they would lose genetic diversity following the MAR relationship (section II.4), with all species having $z_{MAR} = 0.3$ for simplicity (i.e. all species lose genetic diversity at the same rate). For extinct species (100% of their area reduced), we considered genetic diversity loss was 100%. The compound total genetic diversity loss would then just be the sum of those $X_{Tot} = \sum_{i=1}^{1000} X_i$ (Of course, in reality species may vary in their genome-wide diversity average, and we could for instance use Watterson's Θ_W (see section II.2) to scale the total loss of genetic diversity in the ecosystem accounting for different basal level of diversity per species: $\sum_{i=1}^{1000} \Theta_{Wi} X_i$). Interestingly, if we calculate the z of the slope of compound genetic diversity across species in an ecosystem it is much larger than MAR or SAR alone: $z_{compunded} = 0.6$ (Fig. S27).

R. Gillespie, H. Krehenwinkel, D. L. Mahler, F. Massol, C. E. Parent, J. Patiño, B. Peter, B. Week, C. Wagner, M. J. Hickerson, A. Rominger, A unified model of species abundance, genetic diversity, and functional diversity reveals the mechanisms structuring ecological communities. *Mol. Ecol. Resour.* **21**, 2782–2800 (2021).

SUPPLEMENTAL FIGURES

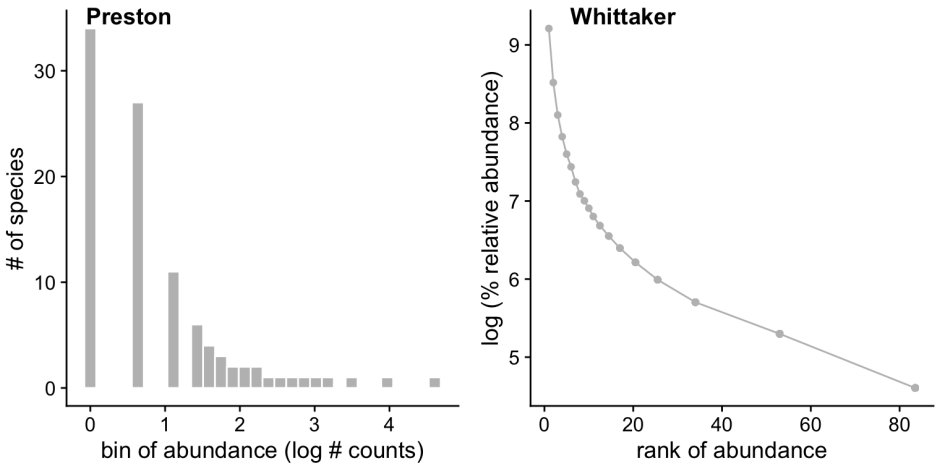

Fig. S1 | Example of typical plots used for species abundance curve studies
Due to their strong skew, Species Abundance Curves are often plotted using the Preston plot (left) where the x axis represents bins of log2 abundances (also referred to as octaves), or using the Whittaker plot (right) where the x axis is the rank of each species in a dataset and y axis the species' relative abundance.

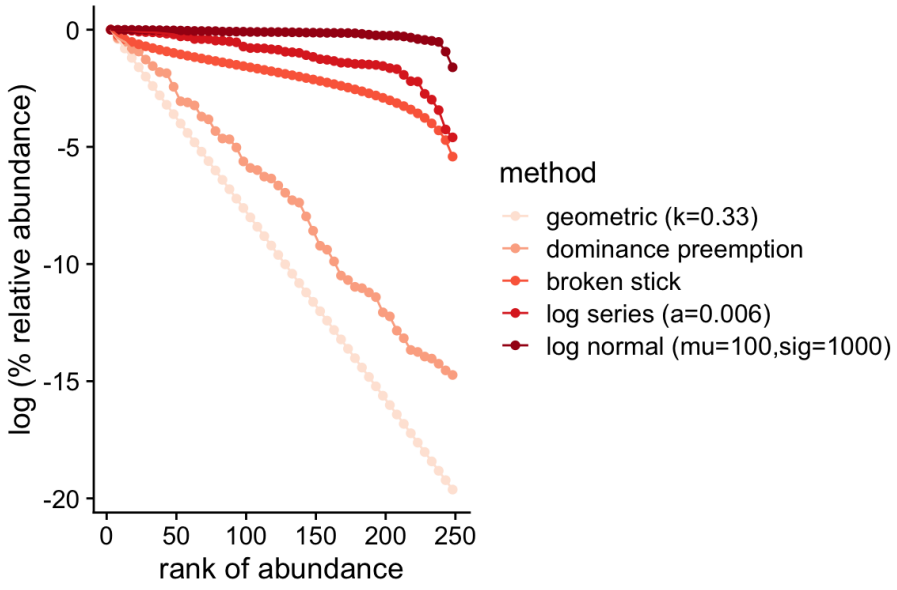

Fig. S2 | Summary of theoretical models of Species Abundance Curves.
Five niche partitioning or statistical models shown in a Whittaker plot. The different models expect different levels of evenness in abundance across the species in the community, from the lowest (geometric series) to the highest (log-normal).

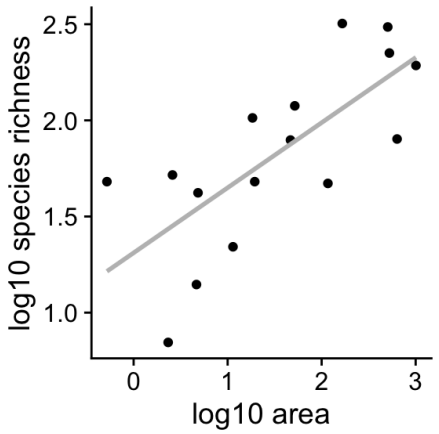

Fig. S3 | Example of a Species-Area Relationship in Galapagos Islands
Classic species richness dataset from the Galapagos Islands (Preston, 1962). It depicts species richness as a function of island area in a log-log plot.

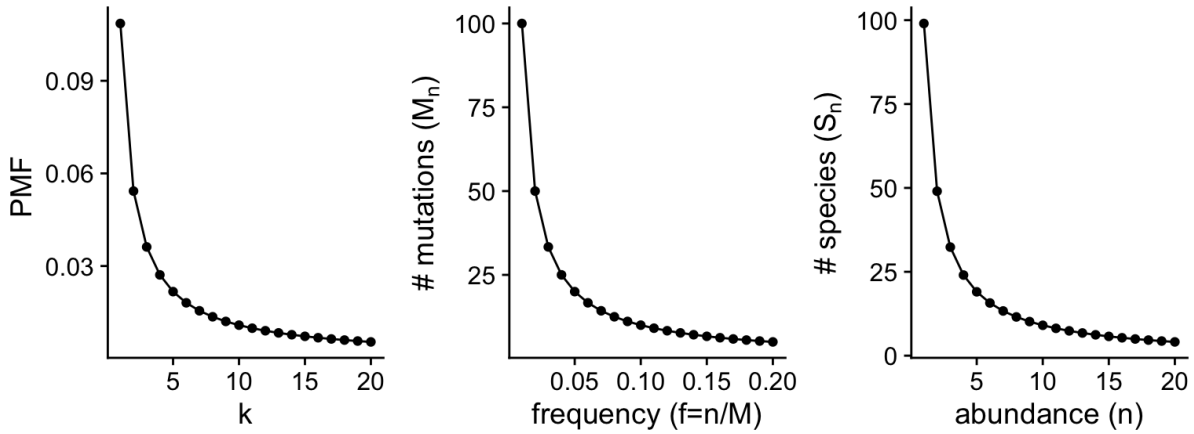

Fig. S4 | Similarity between the Species Abundance Distribution and the Site Frequency Spectrum
Left is the Probability Mass Function of the log-series (p=0.999), center is the SFS (N=100, c=1), and right is the log-series-based abundance of species (alpha=100, N=10000).

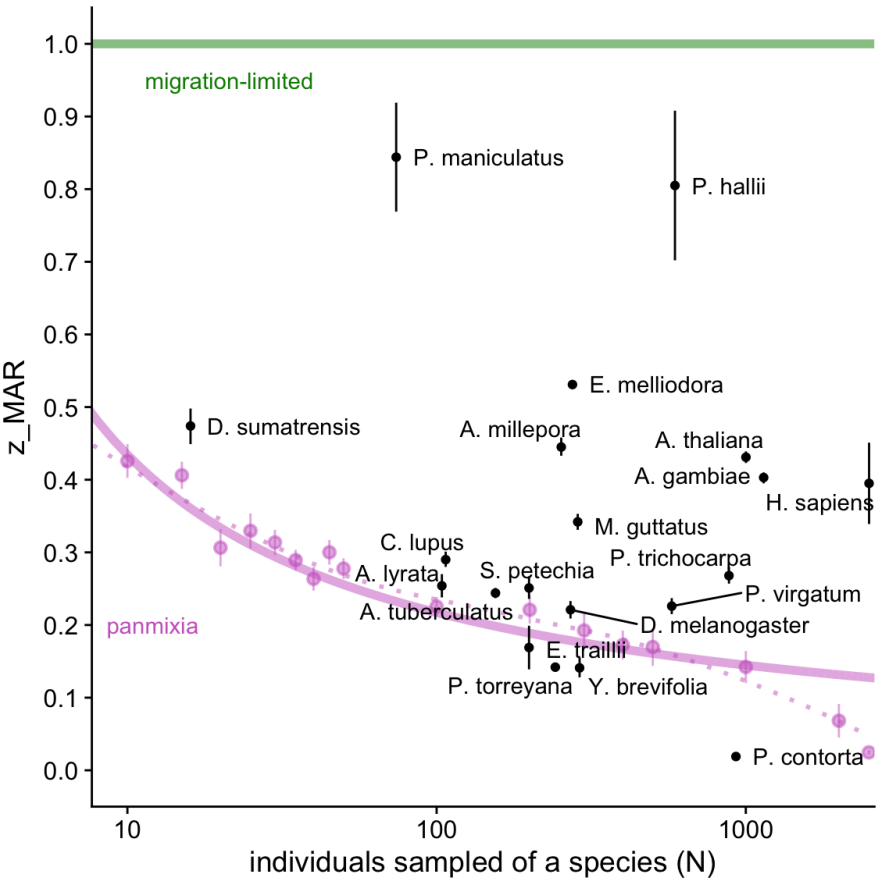

Fig. S5 | Expected ranges of z_{MAR} given sample sizes.
For increasing numbers of individuals sampled, we plot the expected mean z_{MAR} under two theoretical trends of a migration-limited (green) and a panmictic (purple) species (Purple dots indicate averages from SLiM simulations under panmixia to confirm the theoretical trend based on the derivative approach above). In black, z_{MAR} and 95% Confidence Interval of species analyzed in section IV are plotted (see section for details).

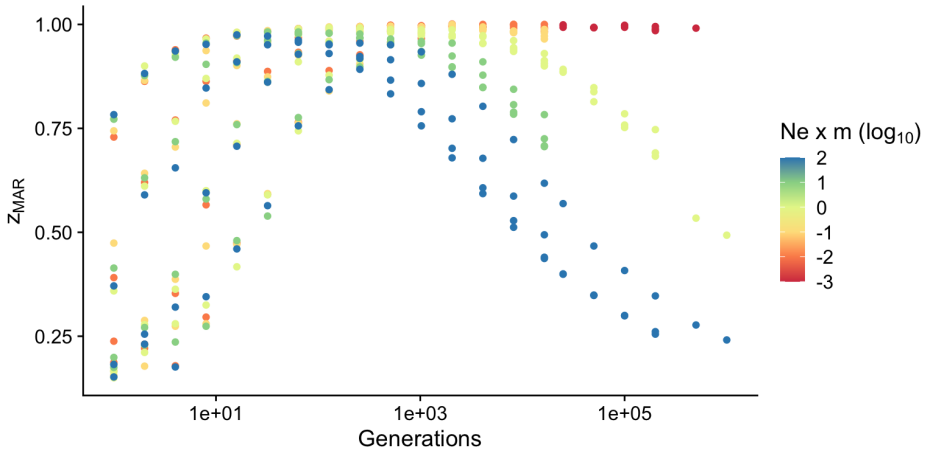

Fig. S6 | msprime 2D deme simulations and the mutations-area relationship
Simulations with different burn-in and migration rates under neutrality, and their corresponding zmar.

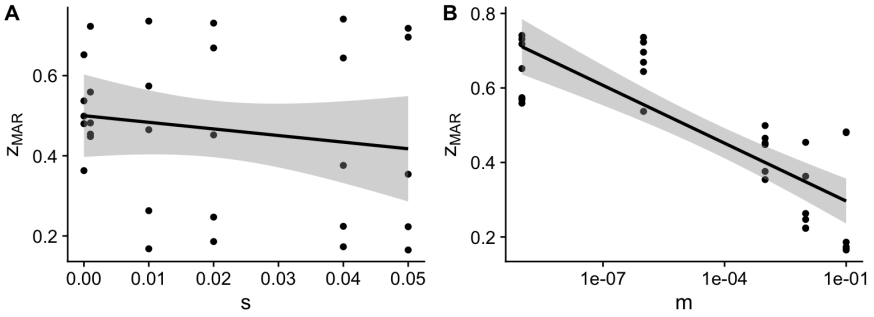

Fig. S7 | SLiM population genetic simulations in 2D with selection and local adaptation
Simulations were carried out with different combinations of migration rates and strength of antagonistic pleiotropic selection at 12 QTLs. (A) Marginal relationship between z_{MAR} with the strength of spatially-varying selection s. (B) Marginal relationship between z_{MAR} with the migration rate m.

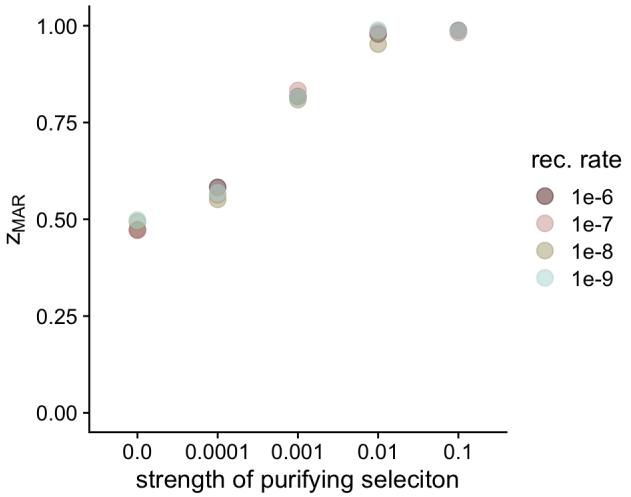

Fig. S8 | SLiM population genetic simulations in 2D with purifying selection
Simulations were carried out with varying strengths of purifying selection (|s| range from 0.0 to 0.1) at coding positions, representing about 29% of the genome. Different values of recombination rate were also used in all pairwise combinations with |s|.

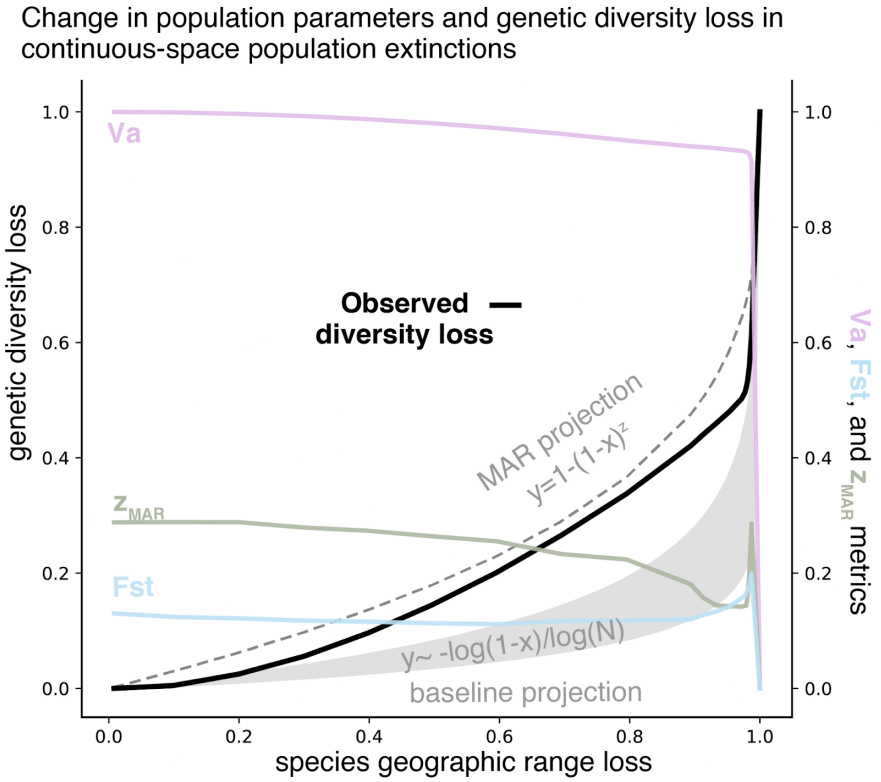

Fig. S9 | Continuous space SLiM population genetic simulations

At 19 timepoints leading up to extinction, 1,000 individuals were sampled randomly in continuous space to quantify diversity loss (black line). The prediction of MAR (dashed line) using the starting z_{MAR} seemed to follow the real trend better than the baseline of just loss of individuals(dashed line). This suggests that even if z_{MAR} varies during the population extinction process, it is relevant to understand genetic loss by area reduction. We also tracked metrics of population structure (z_{MAR}, F_{ST}) and a proxy of adaptive capacity (Va), which showed qualitatively similar patterns as the GWA-based trends (Fig S21).

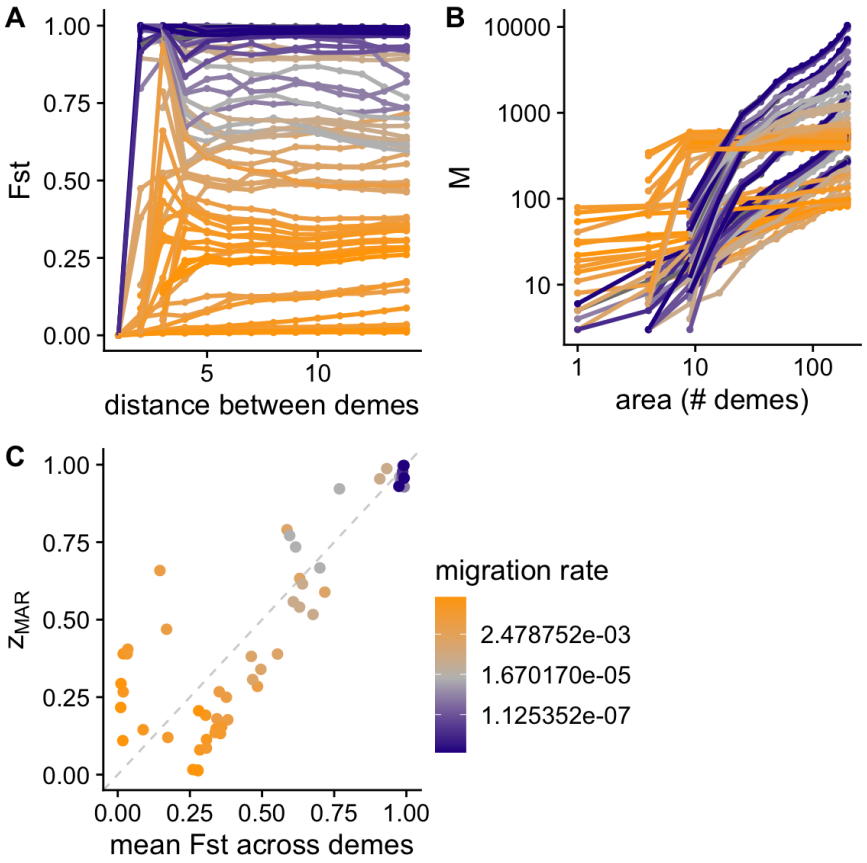

Fig. S10 | SLiM population genetic simulations in 2D comparing F_{ST} and z_{MAR}
Neutral SLiM simulations with different degrees of migration. (A) Hudson's F_{ST} across populations with different area subsamples. Following the expectation of the isolation-by-distance pattern, as the distance between the farthest demes in the subsample increases, F_{ST} becomes larger and saturates at large distances. (B) The mutations-area relationship. (C) Comparison between F_{ST} and z_{MAR}.

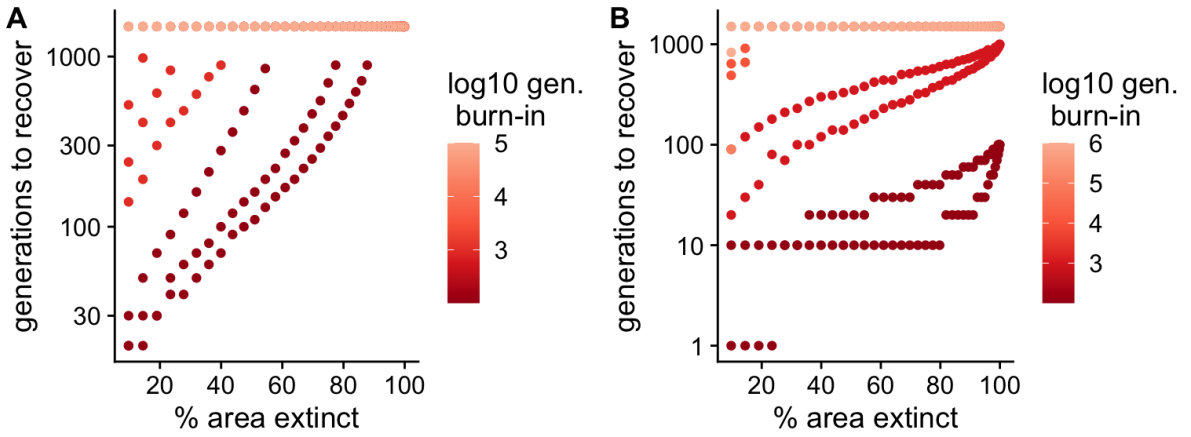

Fig. S11 | 2D stepping-stone msprime simulations with extinction and recovery
(A) Recovery of genetic diversity (number mutations) after loss of a fraction of the population. (B) Recovery of genetic diversity after instantaneous loss of a fraction of the population and consecutive repopulation.
**Simulations with number of generations until recovery that are exceedingly large are assigned a value of 1,500, as none are realistic for current conservation timelines.*

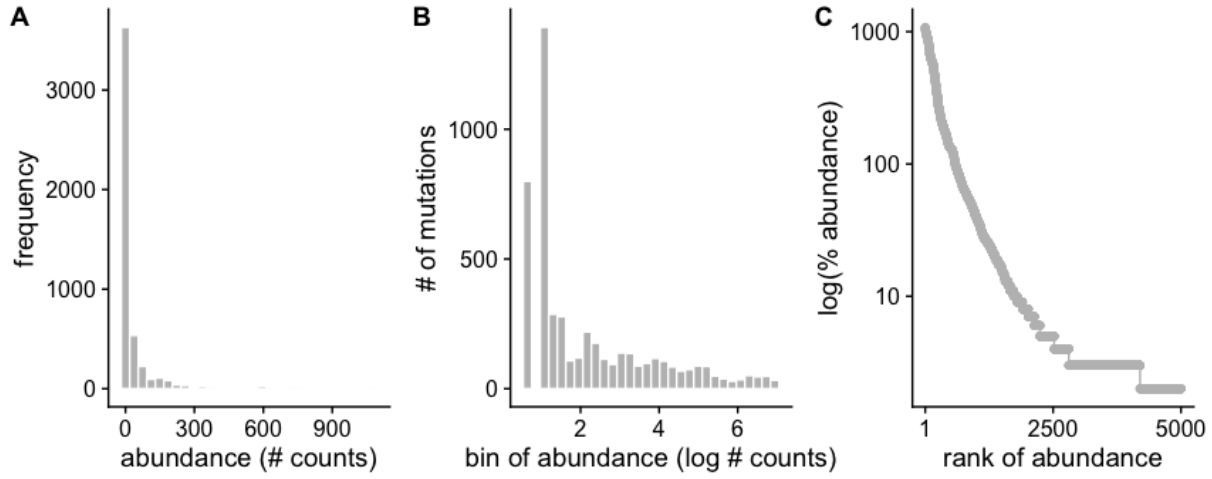

Fig. S12 | Mutation abundance study in A. thaliana
(A) Site Frequency Spectrum (SFS). (B) Preston plot of mutation abundances. (C) Whittaker plot of mutation rank abundances.

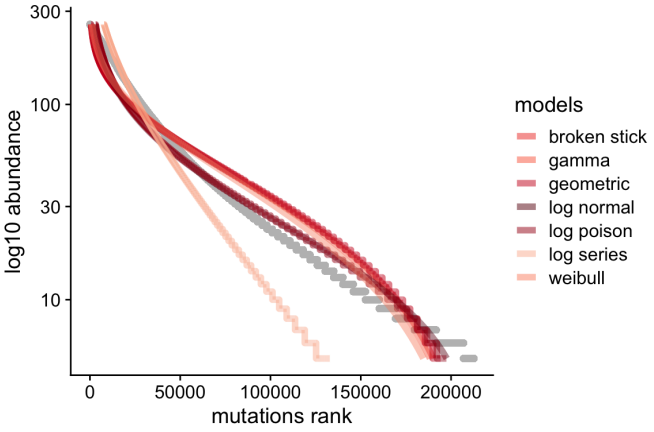

Fig. S13 | Fit of mutation abundance study in A. thaliana with different SAD models
Representative models from Table S3 are plotted along with the observed frequency of 11,769,920 mutations.

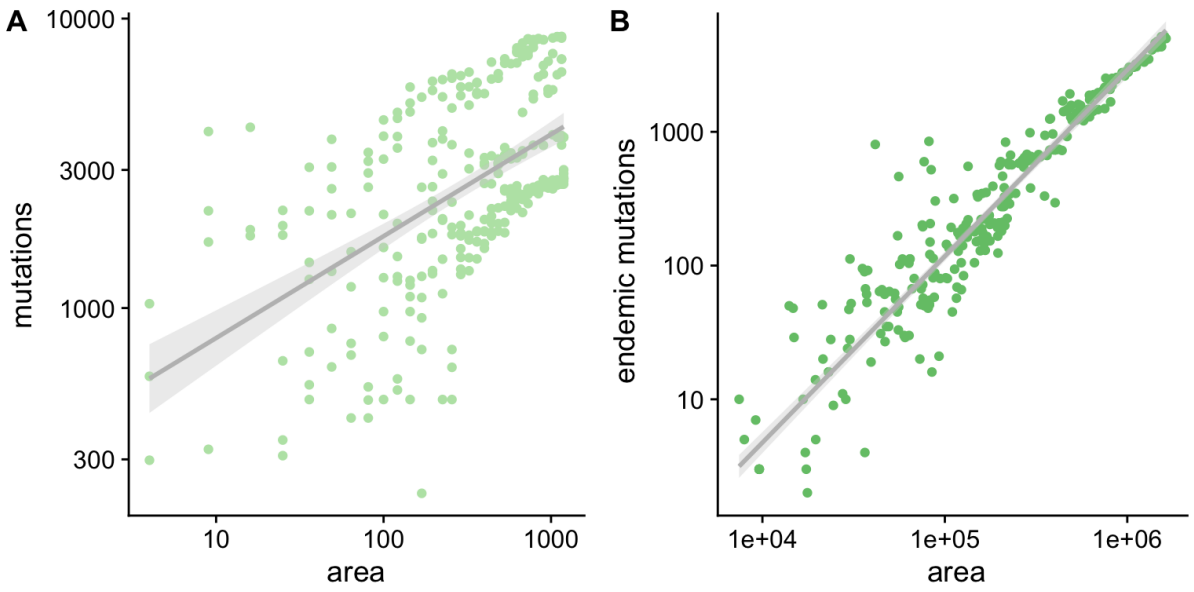

***Fig. S14 | The mutations-area and endemic-mutations-area relationships in* A. thaliana.**
Dividing A. thaliana *native geographic distribution into a 1 degree latitude/longitude grid, square areas with 1 degree side-length to 36 degrees side-length were randomly placed (n=100 for each size) across the distribution, and genetic diversity metrics were computed to produce the (A) Mutations-Area Relationship and (B) Endemic-Mutations Area relationship.*

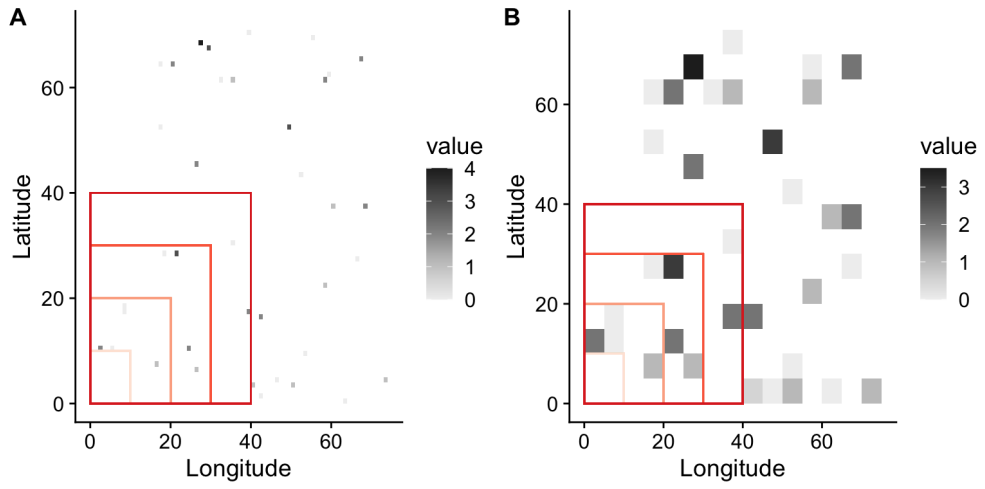

Fig. S15 | Cartoon of raster sampling to build the MAR

Map of mock samples of a species projected into a raster. Grey scale indicates the number of samples per grid cell. Red boxes exemplify the process of spatial subsampling of increasing area to build the MAR relationship. Two example grid sizes were created for illustrative purposes: (A) Small grid size or high spatial resolution. (B) Large grid size or low spatial resolution.

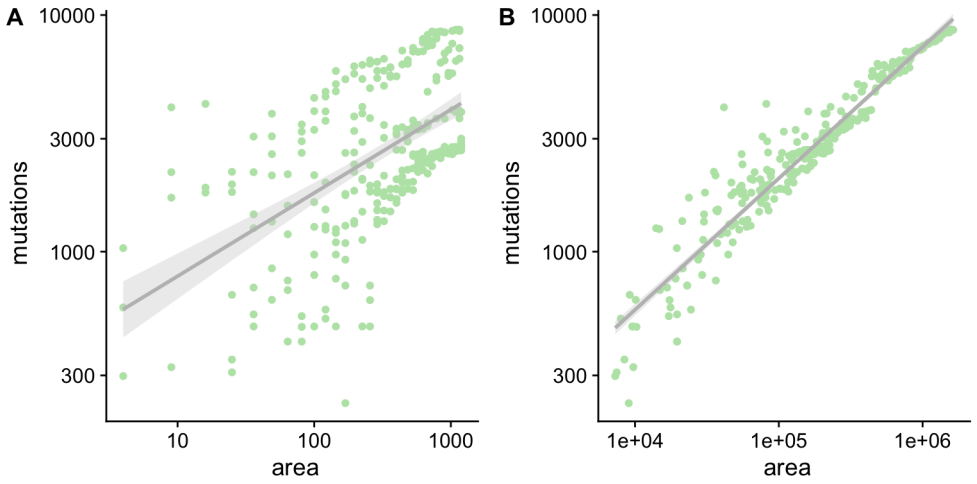

Fig. S16 | MAR comparison with different area calculations.
(A) Using total area, (B) using grid cell sum with at least one sample. For 1 degree latitude/longitude grid cell.

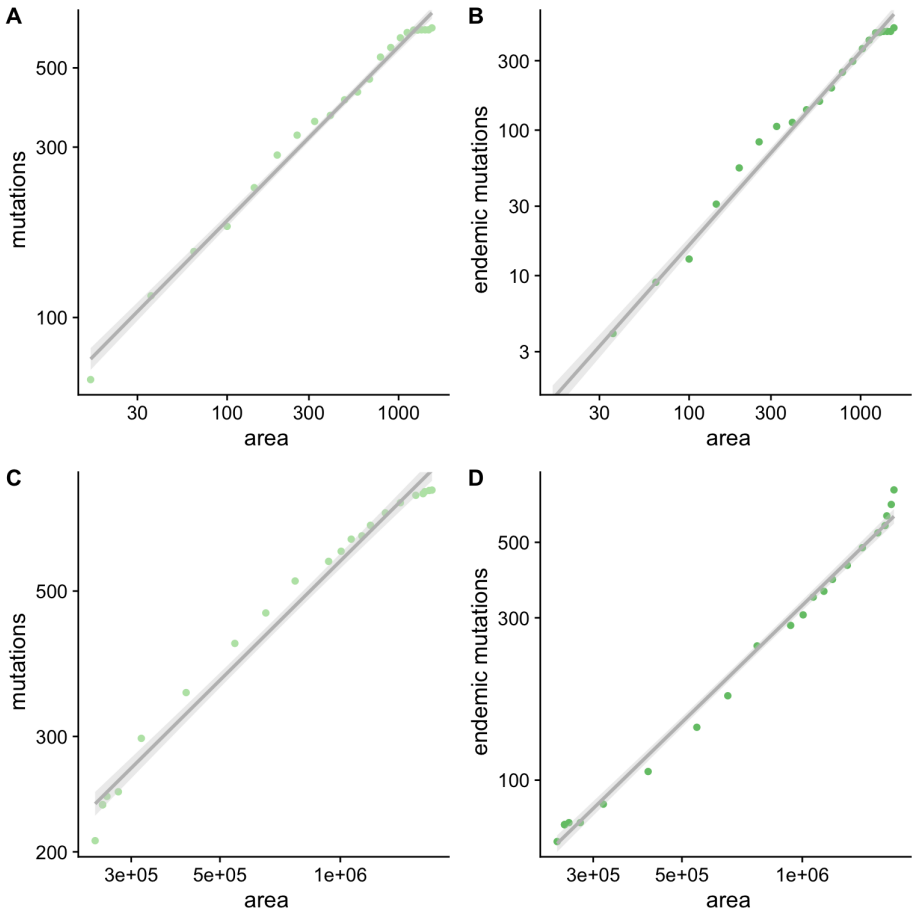

Fig. S17 | MAR and EMAR in Arabidopsis thaliana using outward and inward sampling.
Dividing A. thaliana native distribution in 1 degree lat/long grid, a square area of 1 degree was placed at the median of the sampling range and was expanded iteratively by 1 degree lat/long until all the area of the distribution was covered. (A-B) MAR and EMAR using a typical outward sampling. (C-D) MAR and EMAR using an inward sampling. The latter may not be a common process of sample collection, but it is common for extinction progress.

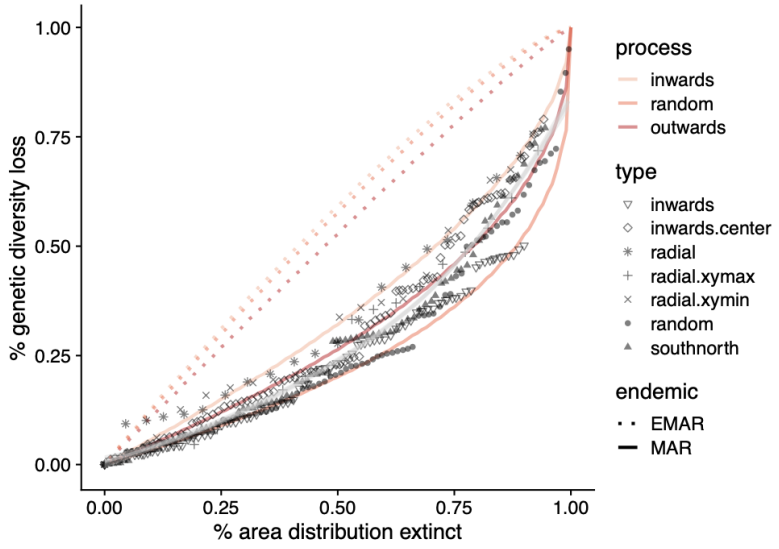

Fig. S18 | Loss of mutations with habitat loss in A. thaliana.
Predictions based on MAR and EMAR functions and in silico extinction stochastic simulations in A. thaliana.

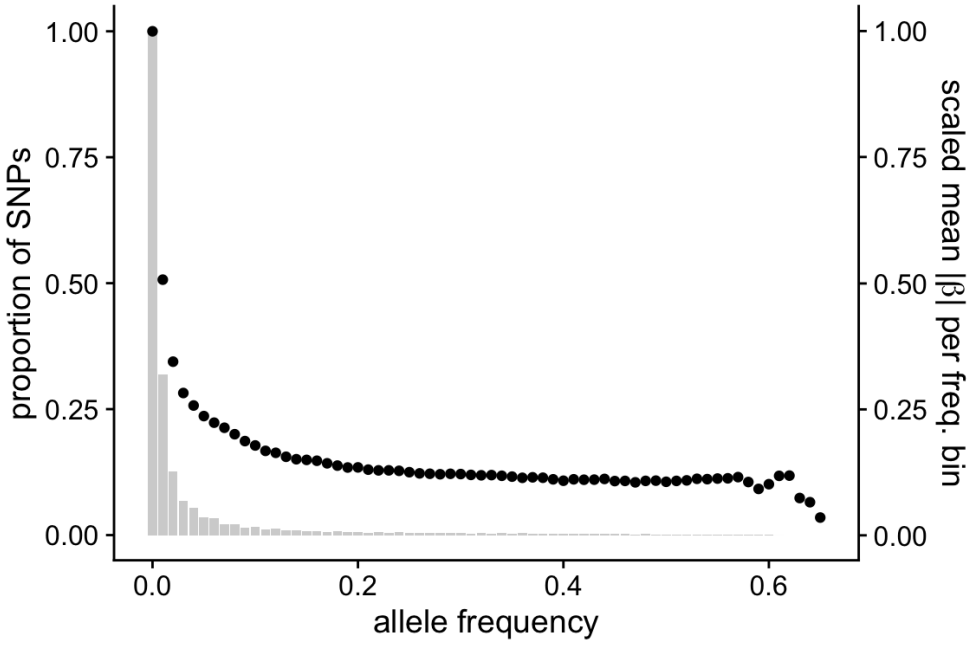

Fig. S19 | Bias of low frequency mutations and effect size for fitness traits in A. thaliana.
Grey bars represent the site frequency spectrum (scaled for visualisation purposes). The black dots represent the mean absolute effects of alleles as estimated from GWAs with 515 accessions scored for fitness traits in 8 outdoor experiments.

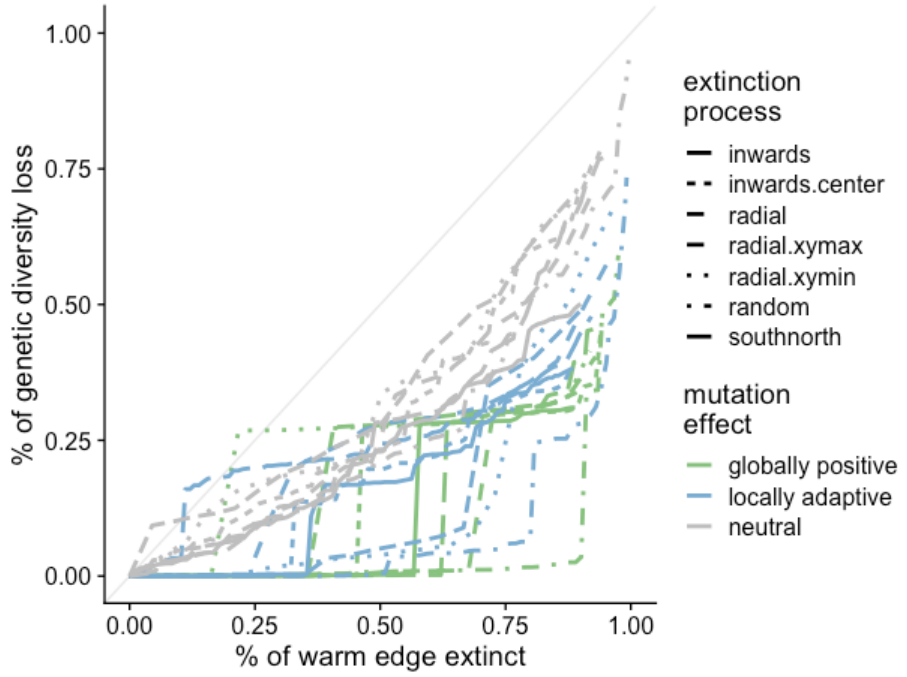

Fig. S20 | Simulations illustrating the potential loss of locally-adaptive mutations in A. thaliana.
Simulations of extinction using multiple patterns of population losses with different subsets of alleles ascertained to show positive associations in fitness GWA in two outdoor experiments (green), positive associations in one environment (e.g. low precipitation) but negative in a second environment (e.g. high precipitation) or vice versa (green). These were compared to a random set (grey).

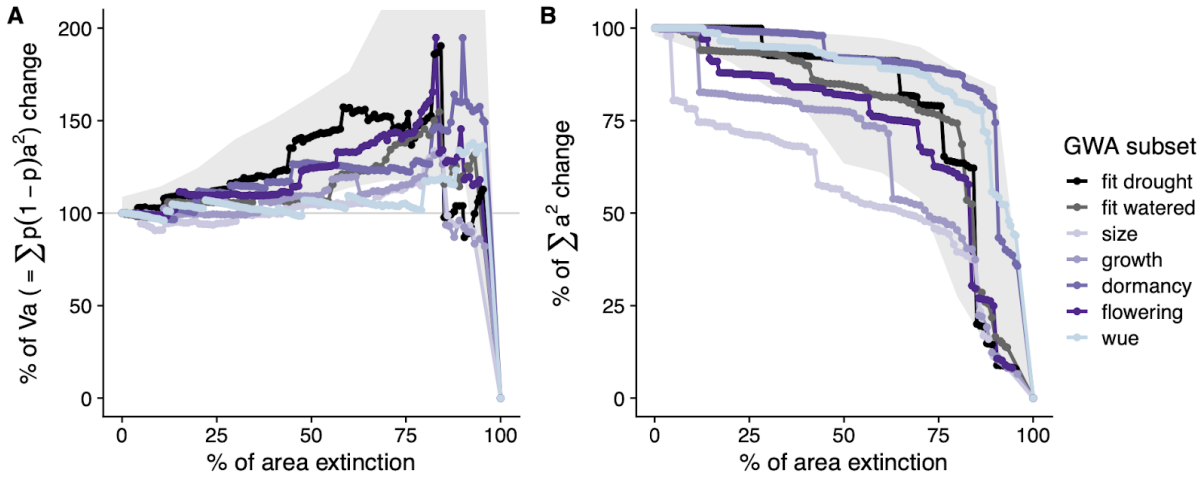

Fig. S21\ Extinction simulations showing proxies of adaptive capacity of A. thaliana.
Using estimated allele effect sizes from 10,000 SNPs in the 1% P-value tails of several Genome-Wide Associations, we show (A) Percentage of change of Va as a proxy of adaptive potential and (B) raw square sum of allele effects to showcase the inflating effect of intermediate frequency alleles. Grey background shape indicates the minimum and maximum boundaries of trajectories created by replicated frequency-matched non-effect sets of SNPs (one per GWA). The trajectories of some effect alleles appear to show faster loss than the non-effect background trajectories.

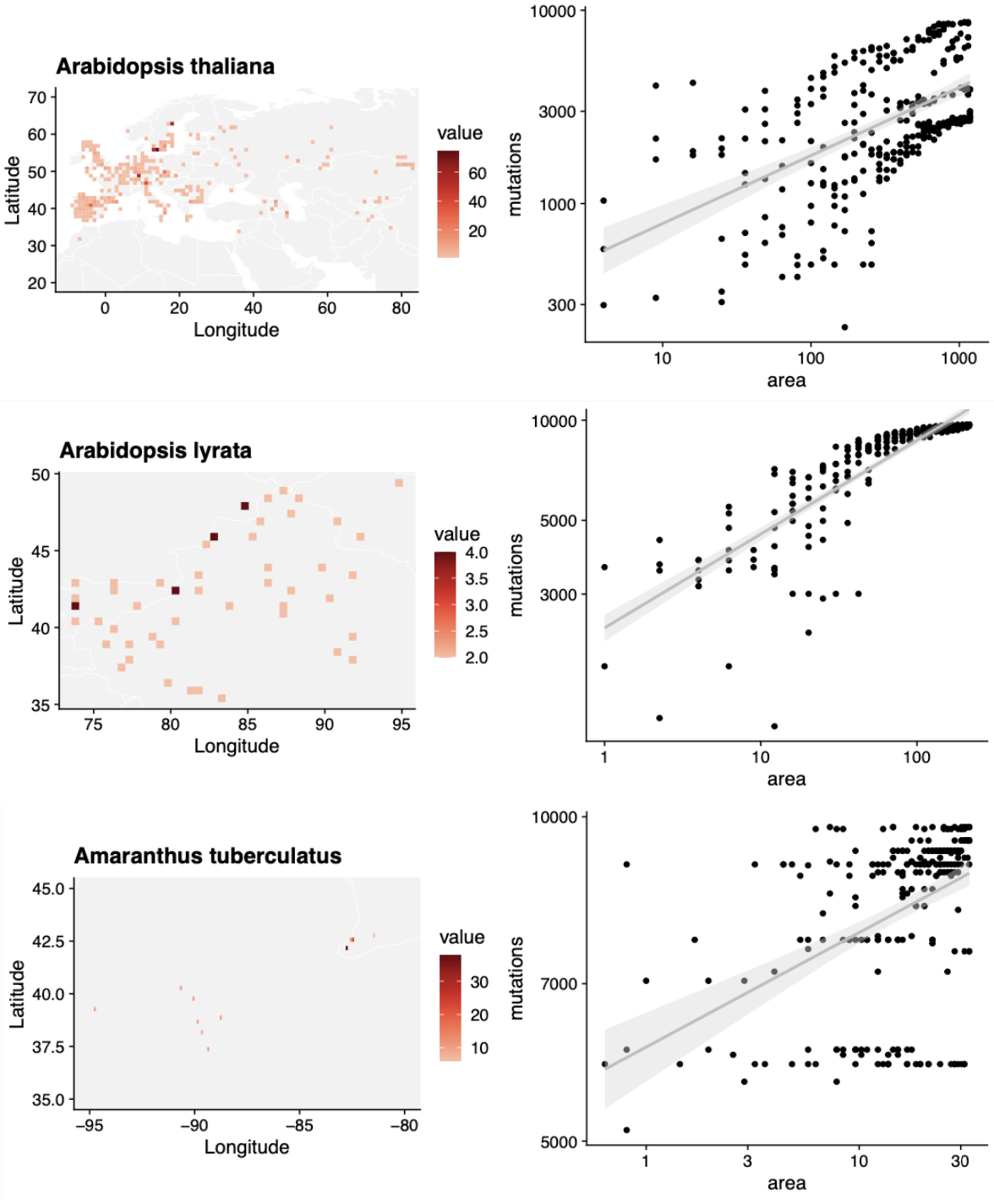
Arabidopsis thaliana
Latitude
Longitude
value
mutations
area
Arabidopsis lyrata
Latitude
Longitude
value
mutations
area
Amaranthus tuberculatus
Latitude
Longitude
value
mutations
area

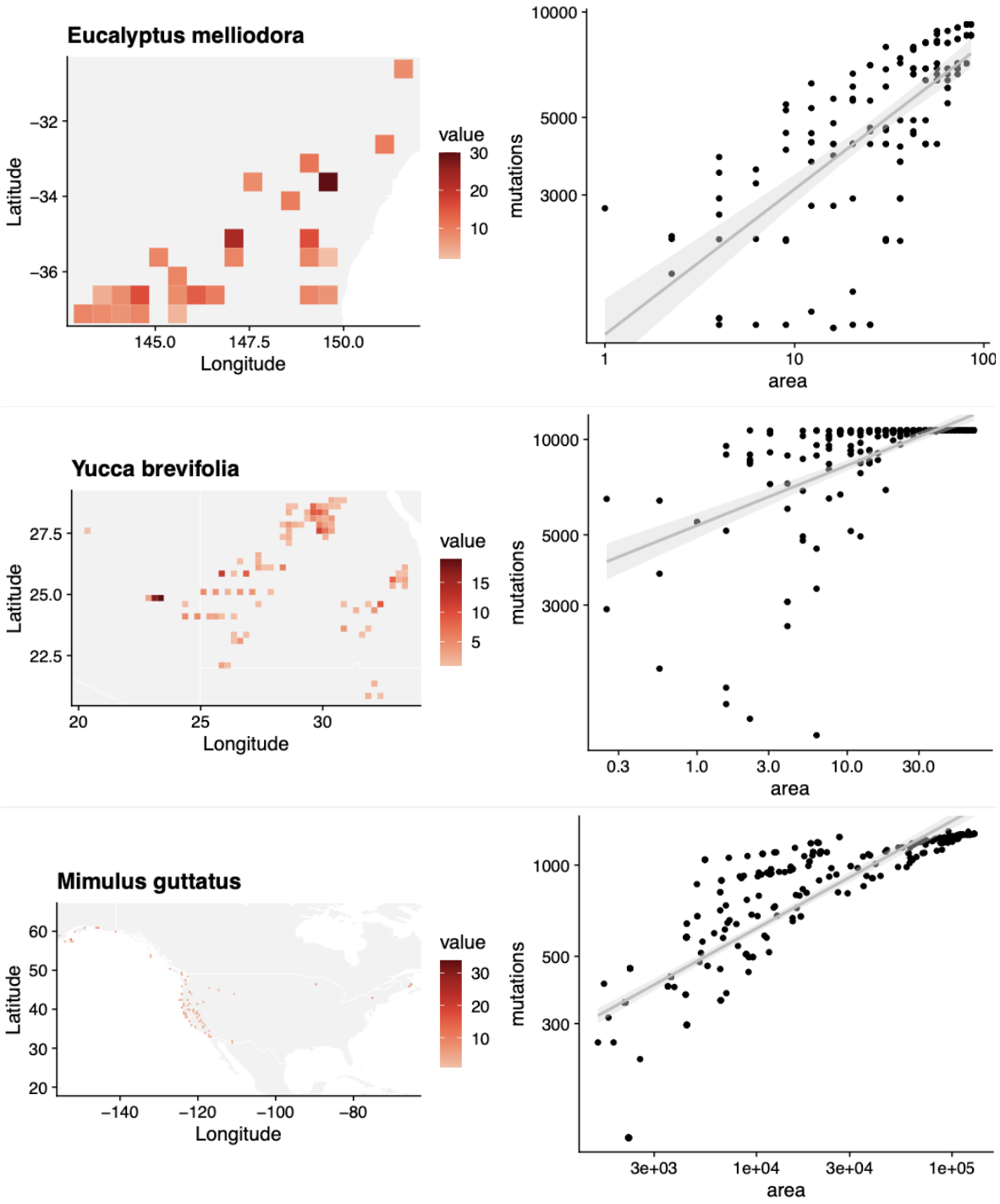
Eucalyptus melliodora
Latitude
−32
−34
−36
145.0
147.5
150.0
Longitude
value
30
20
10
mutations
10000
5000
3000
1
10
100
area
Yucca brevifolia
Latitude
27.5
25.0
22.5
20
25
30
Longitude
value
15
10
5
mutations
10000
5000
3000
0.3
1.0
3.0
10.0
30.0
area
Mimulus guttatus
Latitude
60
50
40
30
20
−140
−120
−100
−80
Longitude
value
30
20
10
mutations
1000
500
300
3e+03
1e+04
3e+04
1e+05
area

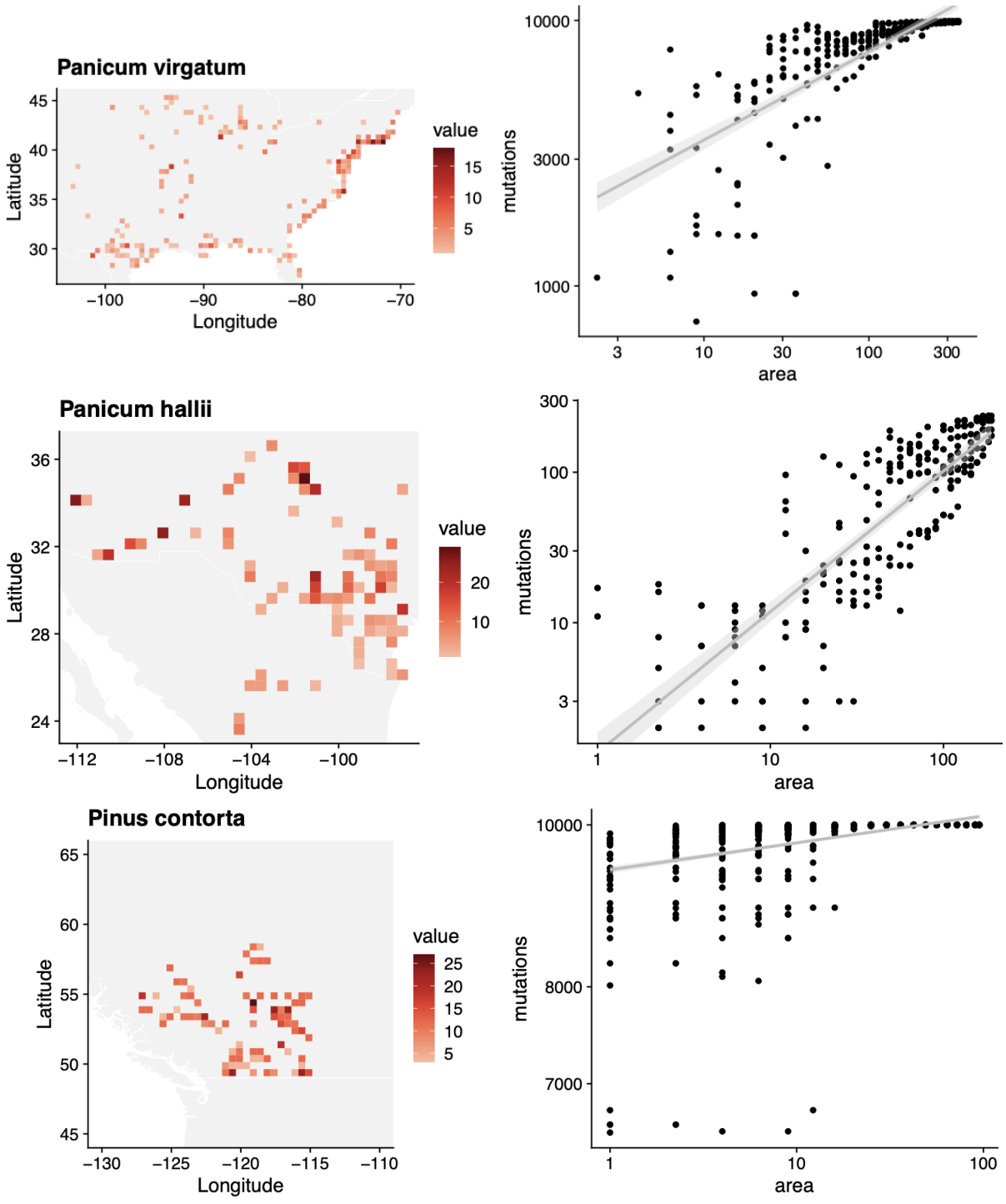
Panicum virgatum
Latitude
Longitude
value
15
10
5
45
40
35
30
−100
−90
−80
−70
mutations
area
10000
3000
1000
3
10
30
100
300
Panicum hallii
Latitude
Longitude
value
20
10
36
32
28
24
−112
−108
−104
−100
mutations
area
300
100
30
10
3
1
10
100
Pinus contorta
Latitude
Longitude
value
25
20
15
10
5
65
60
55
50
45
−130
−125
−120
−115
−110
mutations
area
10000
8000
7000
1
10
100

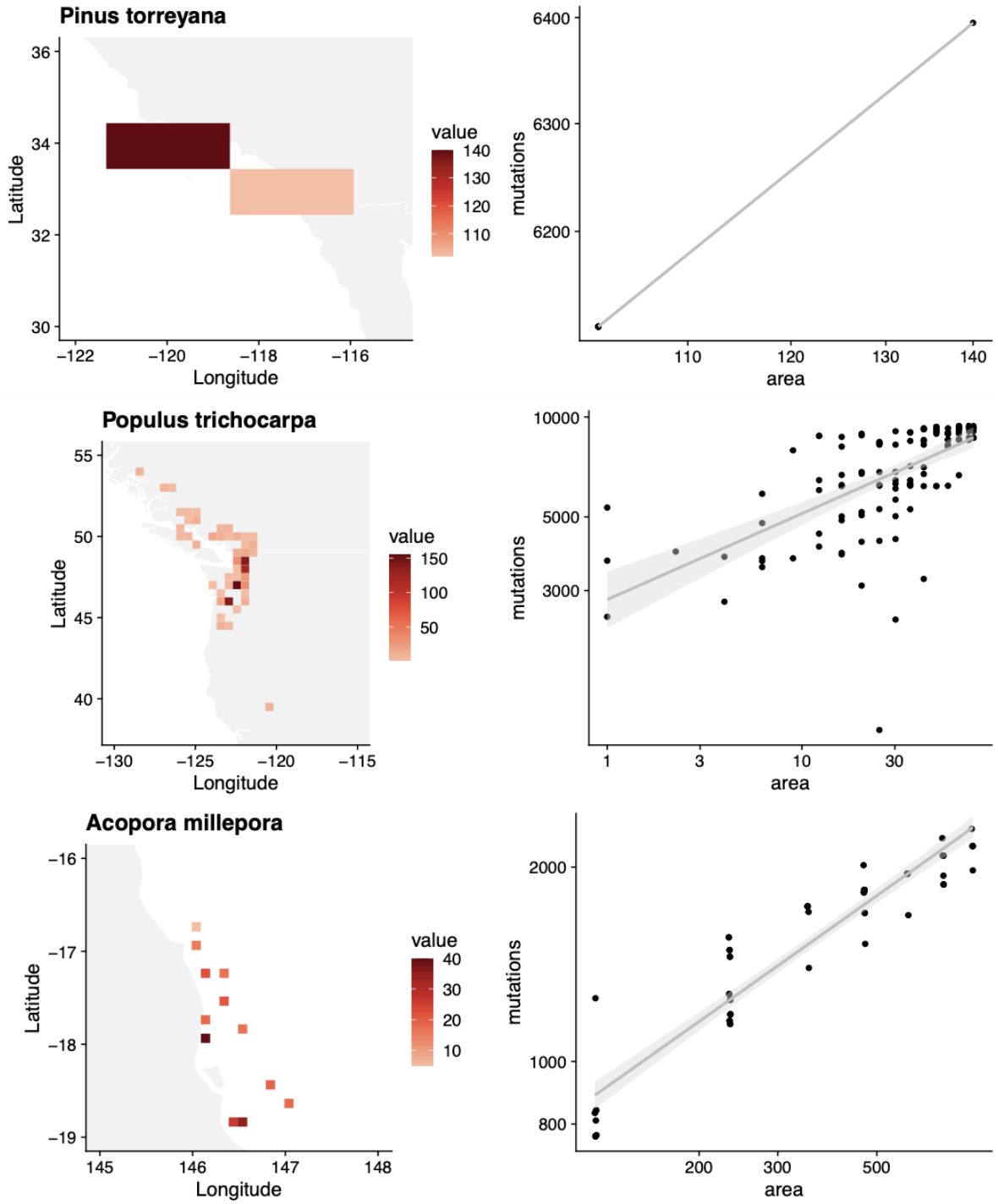
Pinus torreyana
Latitude
Longitude
value
140
130
120
110
mutations
area
Populus trichocarpa
150
100
50
Acopora millepora
40
30
20
10

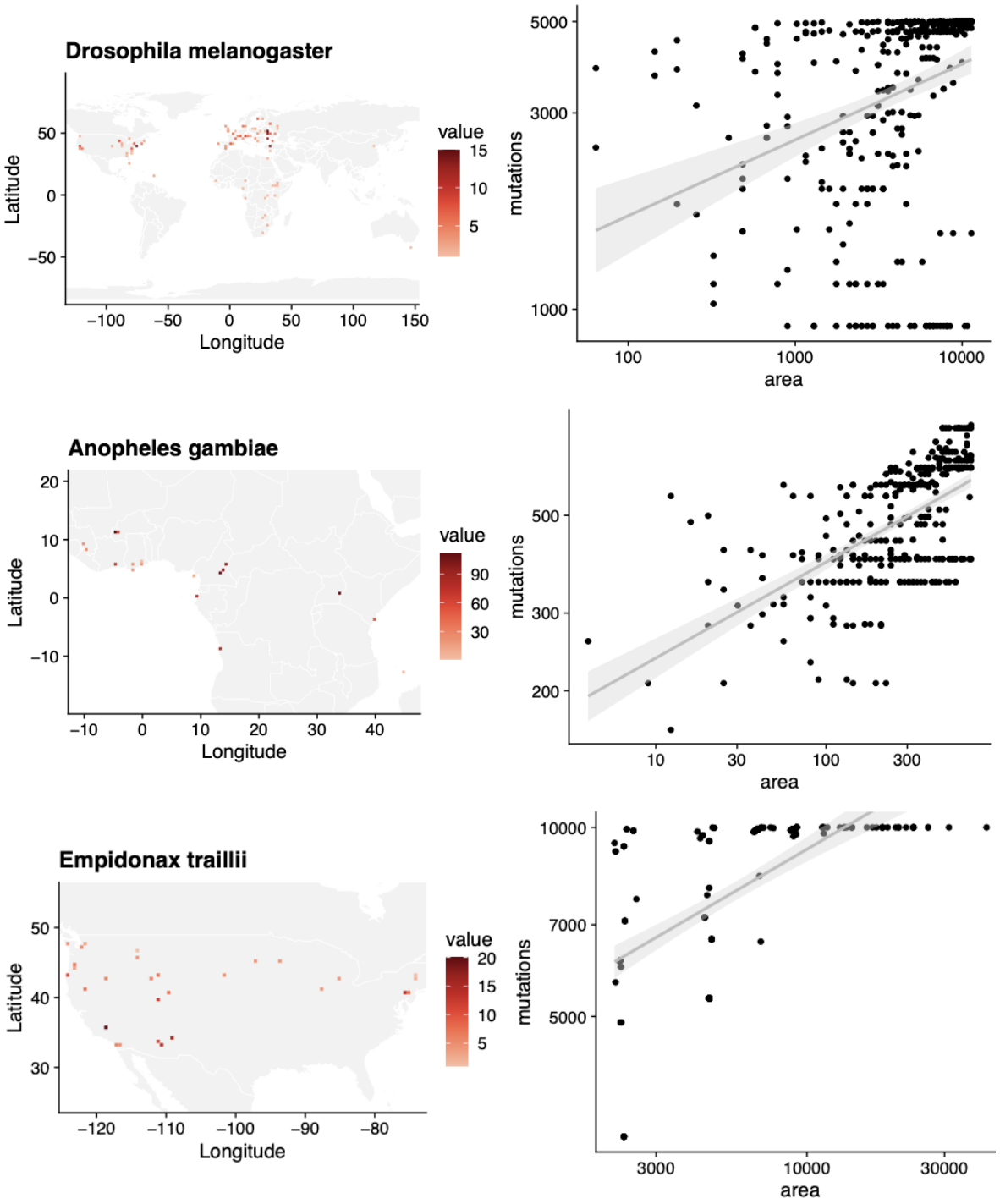
Drosophila melanogaster
Latitude
Longitude
value
mutations
area
Anopheles gambiae
Latitude
Longitude
value
mutations
area
Empidonax traillii
Latitude
Longitude
value
mutations
area

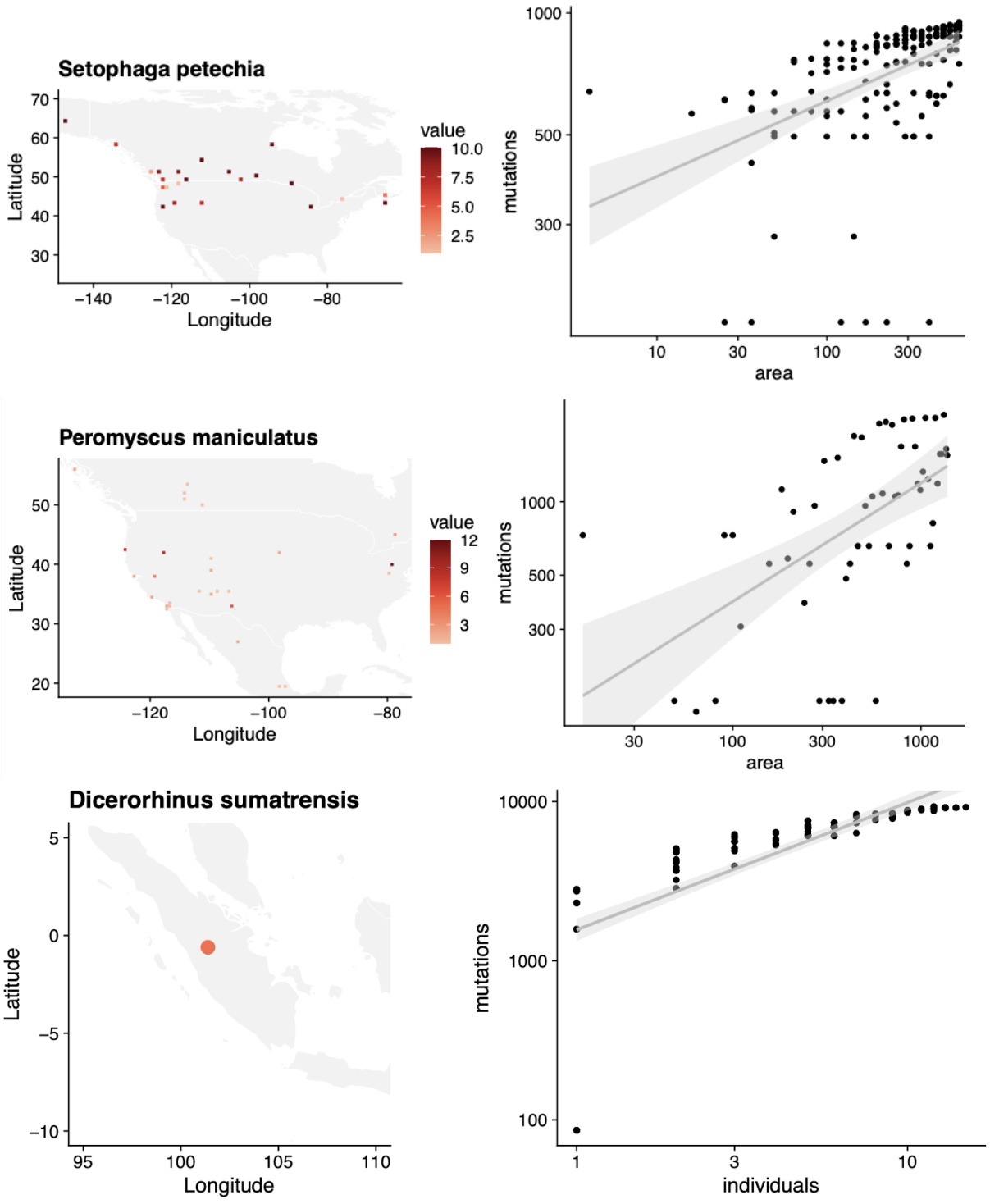
Setophaga petechia
Latitude
Longitude
value
10.0
7.5
5.0
2.5
mutations
area
Peromyscus maniculatus
Latitude
Longitude
value
12
9
6
3
mutations
area
Dicerorhinus sumatrensis
Latitude
Longitude
mutations
individuals

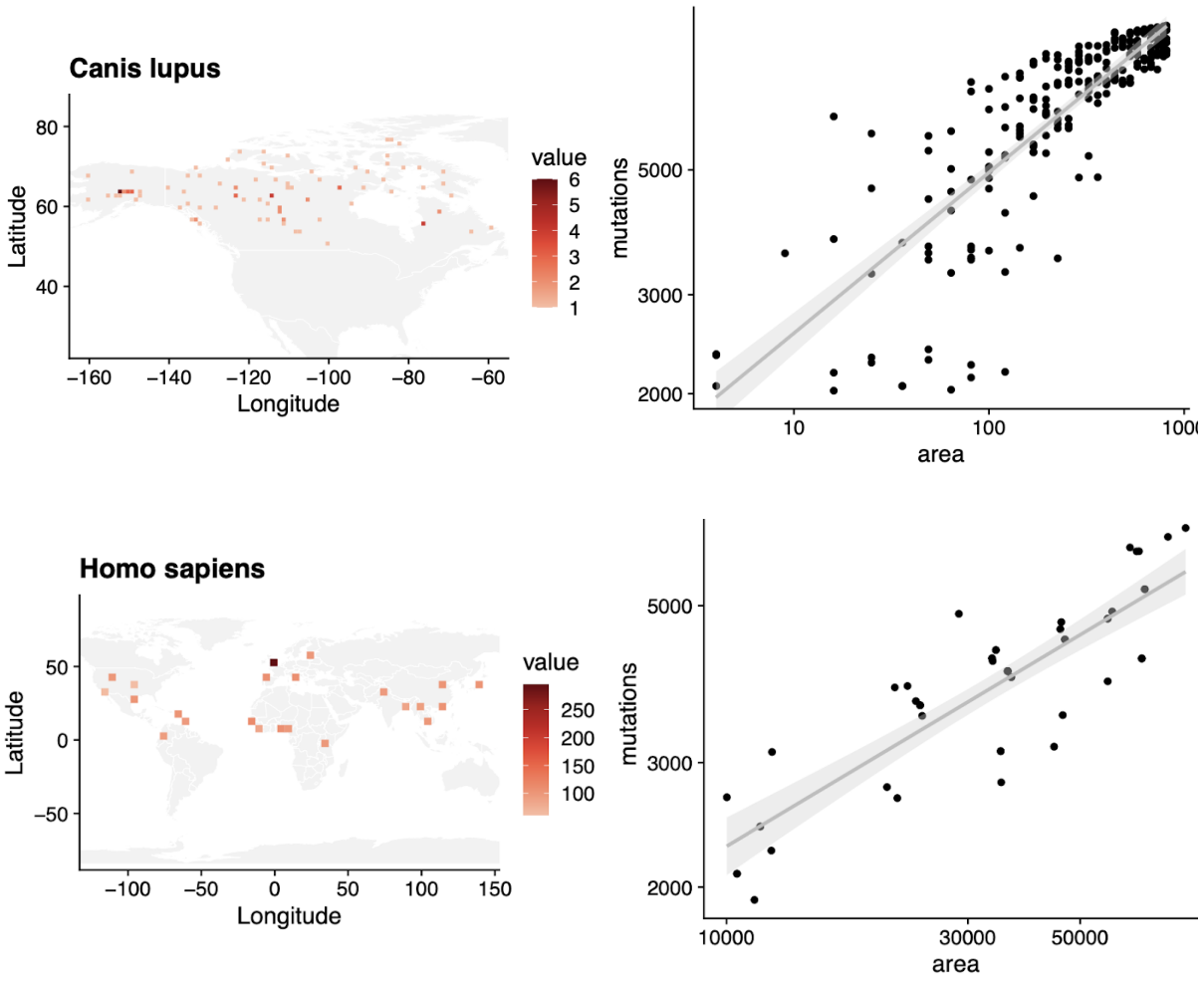

Fig. S22 | MAR summaries across species.
For each species we plot (left) the map of sample density in space and (right) the mutations-area relationship. (The locations of 16 Dicerorhinus sumatrensis are unknown so only Sumatra is shown. Pinus torreyana was only found in two extant populations).

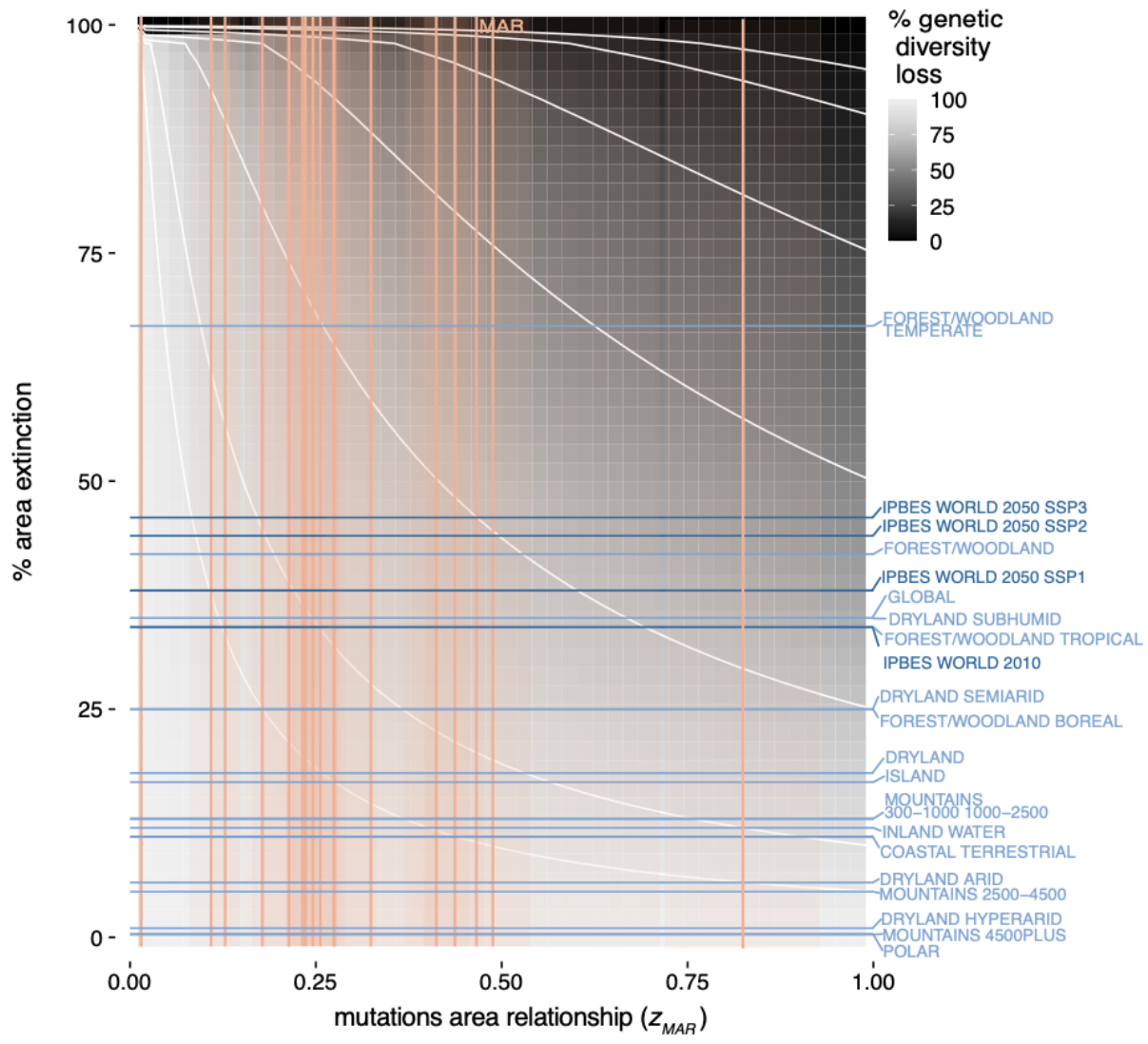

Fig. S23 | The parameter space of genetic diversity loss, extended

(A) The theoretical space of genetic diversity loss. z_{MAR} values and the 95% CI (unscaled, for scaled z^*_{MAR} see Fig. 3 in main text) for each species. Blue horizontal lines correspond to ecosystem transformations from the Millennium Assessment (light blue) and IPBES Assessment (dark blue).

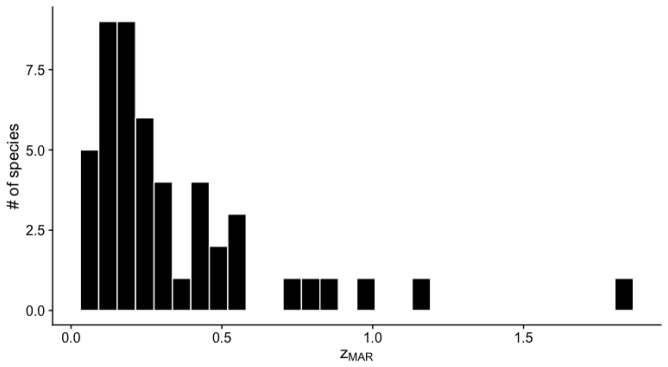

Fig. S24 | z_{MAR} calculated from MESS eco-evolutionary simulations
Using the MESS framework of a mainland-island model with different island sizes, z_{MAR} per species is recovered. The stochastic nature of the simulations results in each species having different abundances and migration histories that change the scaling value. Values were typically around 0.3. Rarely some species had values above 1, which appear could be noisy estimates from recently colonising species in the simulations.

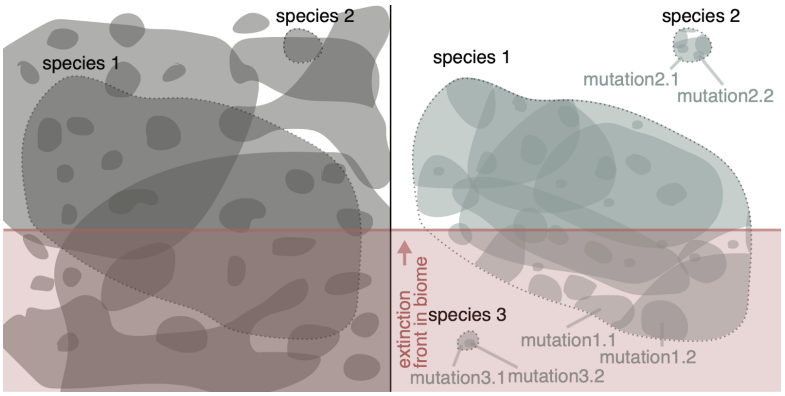

Fig. S25 | Cartoon of nested extinction of species and genetic diversity loss.
An ecosystem with multiple species within it (left), distributed in space, with few species broadly distributed and many narrowly distributed. Moving one level of biological organization lower, mutations within species (right) are also spatially distributed with many narrowly distributed. As extinction happens (red line moving bottom to top), all species below the red line go extinct, but only the mutations within species 1 below the line are lost, while mutations above the line remain. Species 3 has already become extinct, and therefore also all the mutations within it..

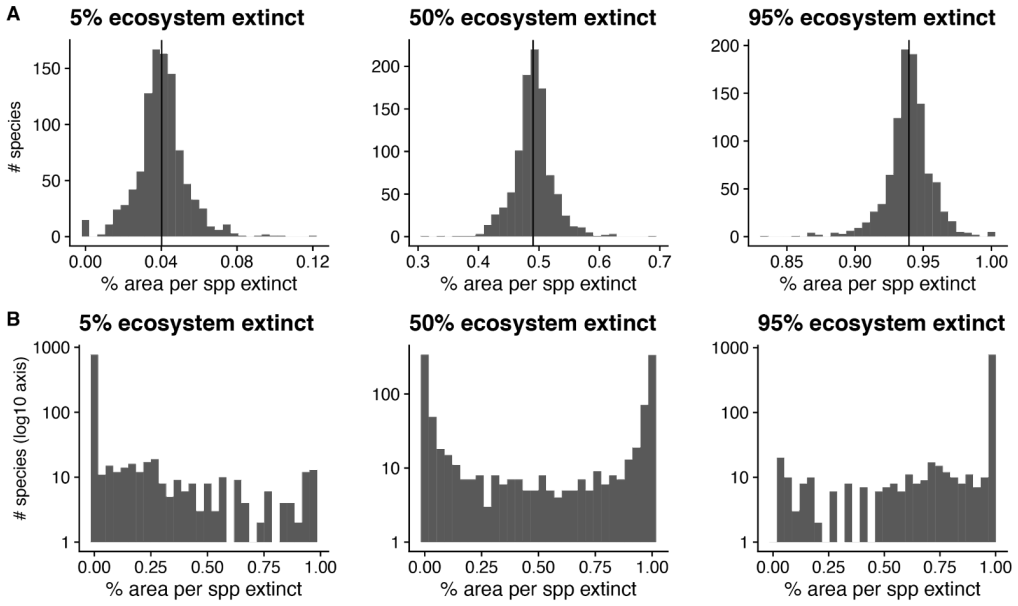

Fig. S26 | The distribution of per-species area lost and total ecosystem extinction with 1000 species
Two ecosystems of 100x100 cells with 1000 species. Species are either randomly distributed in cells (A) or spatially autocorrelated with occupying mostly contiguous cells (B). As the extinction process wipes out part of the ecosystem (snapshots are provided at 5%, 50%, and 95%), the area loss per species (and hence genetic diversity lost) is tracked. In (A) the average area lost per species is roughly the total reduction of the ecosystem, whereas in (B) the distribution is U shaped (note the log-scaled y-axis). While in (B) the mean area lost in the distribution correctly captures the area loss of the ecosystem, per species losses are highly uneven.

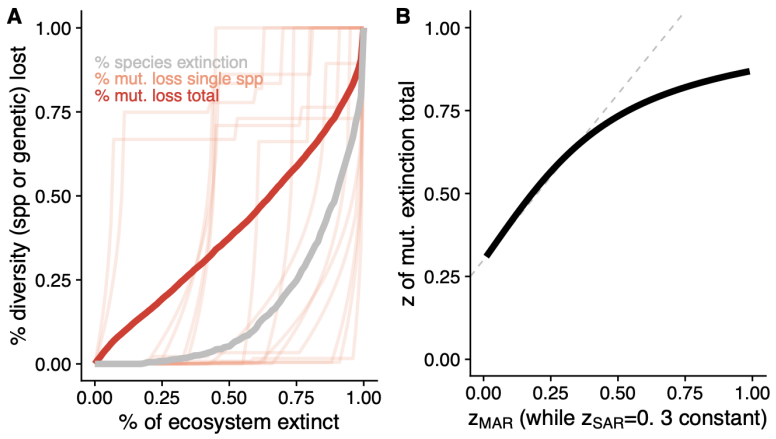

Fig. S27 | Numeric simulation of nested species and genetic diversity loss.
(A) Simulating the extinction of an ecosystem with 1,000 species that follow a log-normal species abundance curve. Extinction of the ecosystem creates a curve of species loss of z~0.3 (grey). Likewise, each species trajectory (light red, 15 species drawn randomly) follows a simulated genetic diversity loss of z_{MAR}~0.3 as they lose area. Because species' geographic distributions are by construction smaller than the whole ecosystem area, those distributed closer to the start of the extinction front lose area first, while those distributed farthest from the extinction front only lose area when the ecosystem is almost completely destroyed. Because genetic diversity loss is both due to complete extinction of species as well as area reduction of extant species, the compound genetic diversity loss curve (red) follows the faster loss dynamics. (B) Holding z_{SAR}=0.3 constant, and varying z_{MAR} in independent simulations shows that the compound genetic diversity across species is close to the sum of both z slopes (the SAR and the MAR), but it saturates at ca. 0.85 (grey dotted line shows z_{MAR} + z_{SAR}).

SUPPLEMENTAL TABLES

Table S1 | msprime population genetic simulations in 2D

Simulations summarised by grouping ranges of the resulting z_{MAR} parameters. The average parameters of the simulations with similar z_{MAR} EW provided. (Acronyms: Nemt = product of effective population size, migration rate, and simulated generations).

z_{MAR}	Samples/deme	Generations	Migration rate	N_emt
0.2 +/- 0.05	2.4	50001.7	0.0271675	5000044.23
0.3 +/- 0.05	20.25	70003	0.0561655	7000075.77
0.4 +/- 0.05	26.5714286	13057.4286	0.04450857	1305497.96
0.5 +/- 0.05	12.9230769	121759.462	0.04017769	752221.743
0.6 +/- 0.05	15.6111111	3218.77778	0.045735	321174.768
0.7 +/- 0.05	35.6842105	35034.8421	0.03395895	143791.614
0.8 +/- 0.05	35.030303	15655.1212	0.03055818	58023.5539
0.9 +/- 0.05	36.5806452	3057.12903	0.0253029	15290.4081
1 +/- 0.05	42.0140845	13625.4085	0.00861178	1798.36141

Table S2 | Linear model explaining z_{MAR} by migration rate and natural selection

Summary table of the linear model $z_{MAR} \sim mig + s + mig:s$

	Estimate	**SE**	**t-value**	***P-value***
intercept	0.3385022	0.0469174	7.214859	0.0000001
mig	-0.0419733	0.0085804	-4.891792	0.0000407
s	-4.693492	1.6290184	-2.881178	0.0076725
mig : s	-0.4998393	0.2426463	-2.059950	0.0491621

Table S3 | AIC values for model fit of common species distribution curves.
For each SAD model, the degrees of freedom and the delta AIC compared to the top model are reported.

Model	dAIC	df
log-Normal	0	2
Poisson	7204.37509	2
Geometric	44267.5475	1
Weibull	45872.3678	2
Gamma	48805.6065	2
Broken Stick	49076.4368	0
UNTB (MTZSM)	168434.181	1
log-Series	168434.726	1

Table S4 | Different SAR curves fit to mutations.
We fit 20 different functions and calculated the variance explained (R2), Pearson's r, and Spearman's rho.

Model	R2	r	rho
Asymptotic regression	0.21825683	0.46717965	0.53510077
Beta-P cumulative	0.22012799	0.46917799	0.53374757
Chapman Richards	0	NA	NA
Cumulative Weibull 3 par.	0.21929646	0.468291	0.53374757
Cumulative Weibull 4 par.	0.21930145	0.46829633	0.53374757
Extended Power model 1	0.21833611	0.46726449	0.53026812
Extended Power model 2	0.21682584	0.46564561	0.53462775
Gompertz	0.16393078	0.40488366	0.45964364
Heleg(Logistic)	0.21929721	0.4682918	0.53531975
Kobayashi	0.22228406	0.47147011	0.53526975
Linear model	0.19579007	0.44248171	0.53510077
Logarithmic	0.20280401	0.45033767	0.53430311
Logistic(Standard)	0.22536996	0.47473146	0.53549765
Monod	0.22500999	0.47435217	0.53579276
Negative exponential	0.22801633	0.47751055	0.53447179
Persistence function 1	0.21929612	0.46829063	0.53501182
Persistence function 2	0.21760028	0.46647645	0.53409266
Power	**0.21929556**	**0.46829004**	**0.53543785**
PowerR	0.21753225	0.46640353	0.53493321
Rational function	0.22072491	0.46981369	0.53451874

Table S5 | The mutations-area relationship (MAR).

Fitted values in a log-log power function between area sampled and mutations discovered.

	Estimate	Std. Error	t value	P	2.5%	97.5%	nls.Est.	nls.2.5%	nls.97.5%
c	494.565432	135.6314588	3.646392	0.0003138	223.3025141	765.8283493	494.5531270	278.1107276	822.829918
z	0.323727	0.0430277	7.523681	0.0000000	0.2376715	0.4097824	0.3237367	0.2430303	0.413162

Table S6 | The endemic-mutations-area relationship (EMAR).

Fitted values in a log-log power function between area sampled and endemic mutations discovered.

	Estimate	Std. Error	t value	P	2.5%	97.5%	nls.Est.	nls.2.5%	nls.97.5%
c	0.0001001	0.0000231	4.337758	1.98e-05	0.0000539	0.0001463	0.0001001	0.0000635	0.0001555
z	1.2411831	0.0165268	75.101442	0.00e+00	1.2081296	1.2742366	1.2412125	1.2096087	1.2737927

Table S7 | MAR built with different area calculations and grid sizes

Grid resolution (deg.)	**z_{MAR} [CI95%] (cell area)**	**z_{MAR}[CI95%] (total area)**
A=N	0.431 (0.423 - 0.439)	NA
0.1	0.435 (0.424 - 0.446)	0.367 (0.281 - 0.454)
0.25	0.454 (0.449 - 0.459)	0.422 (0.376 - 0.467)
0.5	0.488 (0.465 - 0.511)	0.352 (0.152 - 0.551)
1	0.543 (0.529 - 0.558)	0.389 (0.295 - 0.483)
2.5	0.644 (0.6 - 0.688)	0.388 (0.251 - 0.526)
5	0.617 (0.205 - 1.029)	0.403 (-0.204 - 1.011)

Table S8 | Outward and inward MAR and EMAR

The MAR and EMAR relationship computed with inward or outward nested subsampling, calculating area only as those cells with samples.

Relationship	*z*
MAR outwards	0.444 (0.412 - 0.476)
EMAR outwards	1.086 (0.982 - 1.189)
MAR inwards	0.561 (0.524 - 0.597)
EMAR inwards	1.295 (1.192 - 1.399)

Table S9 | MAR for putatively neutral, deleterious, and locally adaptive alleles in Arabidopsis thaliana

SNP set	***z***
neutral	0.324 (0.238 - 0.41)
globally deleterious	0.209 (0.13 - 0.288)
locally adaptive	0.291 (0.217 - 0.365)
globally positive	0.234 (0.137 - 0.332)

Table S10 | The mutations-area relationship across species. Extended Table 1

The Mutations-Area Relationship (MAR) fitted with Area = Individuals and the scaled version. In the main text areas to protect 90% of genetic diversity per species are provided given the scaled z. Here, we also provide the average estimated area based on % of grid cells per species to be transformed from 2015 to 2050 using the LUH² dataset, the area where at least 10% of grid cells will be transformed, and the genetic loss corresponding to those area transformations (see section V.2).*

Species (study)	**SFS** mod [ΔAIC]	**MAR (A=N)** z_N [CI95%]	**LUH² change '50**	**LUH² >10% change '50**	**LUH² extinct '50**	**LUH² >10% extinct '50**
Arabidopsis thaliana (19)	logN (85.8)	0.431 (0.423 - 0.439)	4.58	13.54	1.12	3.43
Arabidopsis lyrata (69)	logN (9592.4)	0.254 (0.238 - 0.27)	0.79	2.64	0.19	0.64
Amaranthus tuberculatus (70)	logN (7317.5)	0.244 (0.237 - 0.251)	4.86	11.13	1.19	2.79
Eucalyptus melliodora (71)	logN (157.5)	0.531 (0.526 - 0.536)	3.82	7.77	0.93	1.92
Yucca brevifolia (85)	logN(33300)	0.141 (0.128 - 0.155)	0.74	0	0.18	0
Mimulus guttatus (72)	logN (580.8)	0.342 (0.331 - 0.353)	3.78	NA	0.92	NA
Panicum virgatum (73)	logN (8345.2)	0.226 (0.215 - 0.237)	8.07	27.65	2	7.47
Panicum hallii (84)	logN (86)	0.983 (0.907 - 1.059)	3.78	11.36	0.92	2.85
Pinus contorta (74)	Wei (19413.7)	0.019 (0.018 - 0.02)	1.95	5.54	0.47	1.36
Pinus torreyana (87)	logN(766156)	0.142 (0.142 - 0.142)	25.4	NA	6.79	NA
Populus trichocarpa (75)	logS (0)	0.268 (0.257 - 0.28)	4.68	17.28	1.14	4.45
Anopheles gambiae (76)	logS (0)	0.221 (0.209 - 0.233)	9.95	21.96	2.48	5.78
Acropora millepora (77)	logN (452.3)	0.403 (0.395 - 0.41)	72.73	84.69	26.79	36.26
Drosophila melanogaster (86)	logN(33300)	0.445 (0.433 - 0.458)	0.95	NA	0.23	NA
Empidonax traillii (78)	Wei (640401.9)	0.169 (0.139 - 0.199)	5.55	15.14	1.36	3.86
Setophaga petechia (79)	ln (67138.5)	0.251 (0.236 - 0.267)	2.83	7.54	0.69	1.86
Peromyscus maniculatus (80)	logN (1449.7)	0.844 (0.769 - 0.919)	5.61	13.68	1.38	3.47
Dicerorhinus sumatrensis (88)	Wei (107864.2)	0.474 (0.449 - 0.498)	0.25	NA	0.06	NA
Canis lupus (82)	logN (85.8)	0.29 (0.28 - 0.301)	0.23	NA	0.06	NA
Homo sapiens (83)	logN (9592.4)	0.395 (0.339 - 0.451)	28.81	40.13	7.83	11.58

Extended acronyms:
logN: log Normal distribution. logS: log Series distribution. Wei: Weibull distribution.

Table S11 | Mean z_{MAR} and other summary statistics across species.

We selected those species that did not show artefacts. See section IV.1 for species removed and explanatory reasons.

	z_{MAR}	z_{MAR} (A=N)	z^*_{MAR} scaled
mean	0.31	0.39	0.27
mean se	0.038	0.053	0.048
median	0.25	0.29	0.18
IQR	0.15	0.19	0.17

Table S12 | Traits, life history, and other characteristics of the analyzed species.

Species	RedList	Known Decline	Kingdom	Reproduction	Pollination	Mobility	AreaRange
Arabidopsis thaliana	NO	NO	Plantae	Selfing	Selfing	Sessile	27337467.4
Arabidopsis lyrata	NO	NO	Plantae	Outcrossing	Vector	Sessile	2791301.4
Amaranthus tuberculatus	LC	NO	Plantae	Outcrossing	Vector	Sessile	804124.8
Eucalyptus melliodora	VU	NO	Plantae	Outcrossing	Wind	Sessile	948699.3
Yucca brevifolia	LC	YES	Plantae	Outcrossing	Vector	Sessile	1213454.4
Mimulus guttatus	LC	NO	Plantae	Outcrossing	Vector	Sessile	25138310.6
Panicum virgatum	LC	NO	Plantae	Outcrossing	Wind	Sessile	6291400.2
Panicum hallii	NO	NO	Plantae	Outcrossing	Wind	Sessile	2188807.4
Pinus contorta	LC	NO	Plantae	Outcrossing	Wind	Sessile	886182.2
Pinus torreyana	CR	YES	Plantae	Outcrossing	Wind	Sessile	30781.95
Populus trichocarpa	LC	NO	Plantae	Outcrossing	Wind	Sessile	1119664.1
Drosophila melanogaster	NO	NO	Animalia	Outcrossing	Activemating	Fly	115208408
Anopheles gambiae	NO	NO	Animalia	Outcrossing	Activemating	Fly	19959809.9
Acropora millepora	NT	YES	Animalia	Outcrossing	Activemating	Fly	26725.9
Empidonax traillii	LC	YES	Animalia	Outcrossing	Activemating	Fly	7027395.2
Setophaga petechia	LC	NO	Animalia	Outcrossing	Activemating	Fly	15172431.15
Peromyscus maniculatus	LC	NO	Animalia	Outcrossing	Activemating	Mobile	22609152.6
Dicerorhinus sumatrensis	CR	YES	Animalia	Outcrossing	Activemating	Mobile	3335605.58
Canis lupus	LC	NO	Animalia	Outcrossing	Activemating	Mobile	19102403.5
Homo sapiens	NA	NA	NA	NA	NA	NA	80763121.8

Table S13 | Association of traits, life history, and other characteristics with z_{MAR}.
Acronyms: NO=not assessed but likely non-threatened, LC=low concern, VU=vulnerable, CR=critically endangered

	Df	Sum Sq	Mean Sq	F value	Pr(>F)
RedList	4	0.0952396	0.0238099	0.5580988	0.7040464
KnownDecline	1	0.0275537	0.0275537	0.6458527	0.4580865
Kingdom	1	0.0011684	0.0011684	0.0273876	0.8750400
Reproduction	1	0.0003238	0.0003238	0.0075890	0.9339612
Pollination	1	0.0375975	0.0375975	0.8812784	0.3909509
Mobility	1	0.1600627	0.1600627	3.7518370	0.1104995
AreaRange	1	0.0174745	0.0174745	0.4095989	0.5503439
Residuals	5	0.2133125	0.0426625	NA	NA

Table S14 | Millennium Ecosystem Assessment land cover transformation.
Changes of ecosystem area pre-21st century. Ecosystem names are repeated for ecosystem sub-classes.
Source: https://www.millenniumassessment.org

System	Area (km^2 $x10^6$)	Earth % surface	Protected areas (%)	Area transformed (%)
MARINE	349.3	68.6	0.3	NA
COASTAL	17.2	4.1	7	NA
- TERRESTRIAL	6	4.1	4	11
- MARINE	11.2	2.2	9	NA
INLAND WATER	10.3	7	12	11
FOREST/WOODLAND	41.9	28.4	10	42
- TROPICAL	23.3	15.8	11	34
- TEMPERATE	6.2	4.2	16	67
- BOREAL	12.4	8.4	4	25
DRYLAND	59.9	40.6	7	18
- HYPERARID	9.6	6.5	11	1
- ARID	15.3	10.4	6	5
- SEMIARID	22.3	15.3	6	25
- SUBHUMID	12.7	8.6	7	35
ISLAND	7.1	4.8	17	17
- STATES	4.7	3.2	18	21
MOUNTAINS	35.8	24.3	14	12
- 300-1000	13	8.8	11	13
- 1000-2500	11.3	7.7	14	13
- 2500-4500	9.6	6.5	18	6
- 4500+	1.8	1.2	22	0.3
POLAR	23	15.6	42	0.38
CULTIVATED	35.3	23.9	6	47
- PASTURE	0.1	0.1	4	11
- CROPLAND	8.3	5.7	4	62
- MIXED	26.9	18.2	6	43
URBAN	3.6	2.4	0	100
GLOBAL	510	NA	4	38

Table S15 | IPBES land cover transformation.
Source: https://ipbes.net

Region	Area(Mkm2)	MSA_2010	MSA_2050_SSP2	MSA_2050_SSP1	MSA_2050_SSP3
North America	20	65	56	NA	NA
Central and South America	18	65	53	NA	NA
Middle East and Northern Africa	11	81	77	NA	NA
Sub-Saharan Africa	24	70	56	NA	NA
Western and Central Europe	6	37	29	NA	NA
Russian region and Central Asia	21	73	65	NA	NA
South Asia	5	44	35	NA	NA
China region	11	56	49	NA	NA
Southeast Asia	7	55	43	NA	NA
Japan, Korea and Oceania	8	71	57	NA	NA
Polar	2	96	91	NA	NA
World	132	66	56	62	54

Table S16 | Land Use Harmonization 2 from 1850 to 2015
Source: https://luh.umd.edu/data.shtml

	Area %
Primary forest transformed	43
Primary non-forest transformed	50

Table S17 | IUCN Red List categories of extinction risk and number of species.
Source: www.iucnredlist.org, July 2022. Number of mammals, amphibians, birds, and plants evaluated by the IUCN.

Category	min. % area reduction (A2-4criteria)	A1	A2-4	B1	B2	C1	C2	D	E	Decreasing population trend	Nspp
EX	~100%	0	**0**	0	0	0	0	0	0	-	452
EX?	~100%	0	**51**	385	472	5	40	236	0	-	782
CEN	80%	136	**916**	3096	2765	147	798	897	0	**61.4%**	5339
EN	50%	149	**1621**	6895	7193	173	577	411	0	**63.1%**	11475
VU	30%	492	**2240**	3976	4138	167	425	0	0	**44.8%**	11001
LR/NT	20-25%	28	**1688**	1201	1397	154	326	0	0	**49.8%**	5292
LC/DD	?	0	**0**	0	0	0	0	0	0	**15%**	48460

Table S18 | Estimates of average expected genetic loss for different ecosystems.

Assuming ecosystem transformation approximately translates into average species distribution reduction, and using the ranges of z_{MAR} from Table 1 of the main text, we project the average genetic loss using the Mutations Area Relationship.

System	*Area transformed (%)*	*Genetic loss % (mean z based)*	*Genetic loss % (min z based)*	*Genetic loss % (max z based)*
COASTAL TERRESTRIAL	*11*	*3.2*	*0.9*	*9*
INLAND WATER	*11*	*3.2*	*0.9*	*79.7*
FOREST/WOODLAND	*42*	*14.0*	*4*	*35.8*
FOREST/WOODLAND TROPICAL	*34*	*10.5*	*3*	*28.7*
FOREST/WOODLAND TEMPERATE	*67*	*26.5*	*7.9*	*59.4*
FOREST/WOODLAND BOREAL	*25*	*7.7*	*2.1*	*20.9*
DRYLAND	*18*	*5.4*	*1.5*	*14.9*
DRYLAND HYPERARID	*1*	*0.3*	*0.1*	*0.8*
DRYLAND ARID	*5*	*1.4*	*0.4*	*4.1*
DRYLAND SEMIARID	*25*	*7.7*	*2.1*	*20.9*
DRYLAND SUBHUMID	*35*	*11.3*	*3.2*	*29.6*
ISLAND	*17*	*5.0*	*1.4*	*14.1*
MOUNTAINS	*12*	*3.5*	*0.9*	*9.9*
MOUNTAINS 300-1000	*13*	*3.8*	*1*	*10.7*
MOUNTAINS 1000-2500	*13*	*3.8*	*1*	*10.7*
MOUNTAINS 2500-4500	*6*	*1.7*	*0.5*	*4.9*
MOUNTAINS 4500+	*0.3*	*0.1*	*0*	*0.2*
POLAR	*0.4*	*0.1*	*0*	*0.3*
GLOBAL	*38*	*12.4*	*3.5*	*32.2*

References and Notes

1. S. Díaz, J. Settele, E. S. Brondízio, H. T. Ngo, J. Agard, A. Arneth, P. Balvanera, K. A. Brauman, S. H. M. Butchart, K. M. A. Chan, L. A. Garibaldi, K. Ichii, J. Liu, S. M. Subramanian, G. F. Midgley, P. Miloslavich, Z. Molnár, D. Obura, A. Pfaff, S. Polasky, A. Purvis, J. Razzaque, B. Reyers, R. R. Chowdhury, Y.-J. Shin, I. Visseren-Hamakers, K. J. Willis, C. N. Zayas, Pervasive human-driven decline of life on Earth points to the need for transformative change. *Science* **366**, eaax3100 (2019). doi:10.1126/science.aax3100 Medline

2. Intergovernmental Science-Policy Platform on Biodiversity and Ecosystem Services (IPBES), *The Global Assessment Report on Biodiversity and Ecosystem Services*, E. S. Brondizio, J. Settele, S. Diaz, H. T. Ngo, Eds. (IPBES Secretariat, Bonn, 2019).

3. J. J. Wiens, Climate-related local extinctions are already widespread among plant and animal species. *PLOS Biol.* **14**, e2001104 (2016). doi:10.1371/journal.pbio.2001104 Medline

4. See supplementary materials and methods.

5. C. Parmesan, Ecological and evolutionary responses to recent climate change. *Annu. Rev. Ecol. Evol. Syst.* **37**, 637–669 (2006). doi:10.1146/annurev.ecolsys.37.091305.110100

6. M. Lynch, J. Conery, R. Burger, Mutation accumulation and the extinction of small populations. *Am. Nat.* **146**, 489–518 (1995). doi:10.1086/285812

7. D. Spielman, B. W. Brook, R. Frankham, Most species are not driven to extinction before genetic factors impact them. *Proc. Natl. Acad. Sci. U.S.A.* **101**, 15261–15264 (2004). doi:10.1073/pnas.0403809101 Medline

8. W. Steffen, K. Richardson, J. Rockström, S. E. Cornell, I. Fetzer, E. M. Bennett, R. Biggs, S. R. Carpenter, W. de Vries, C. A. de Wit, C. Folke, D. Gerten, J. Heinke, G. M. Mace, L. M. Persson, V. Ramanathan, B. Reyers, S. Sörlin, Planetary boundaries: Guiding human development on a changing planet. *Science* **347**, 1259855 (2015). doi:10.1126/science.1259855 Medline

9. L. Laikre, S. Hoban, M. W. Bruford, G. Segelbacher, F. W. Allendorf, G. Gajardo, A. G. Rodríguez, P. W. Hedrick, M. Heuertz, P. A. Hohenlohe, R. Jaffé, K. Johannesson, L. Liggins, A. J. MacDonald, P. OrozcoterWengel, T. B. H. Reusch, H. Rodríguez-Correa, I. M. Russo, N. Ryman, C. Vernesi, Post-2020 goals overlook genetic diversity. *Science* **367**, 1083–1085 (2020). doi:10.1126/science.abb2748 Medline

10. S. Díaz, N. Zafra-Calvo, A. Purvis, P. H. Verburg, D. Obura, P. Leadley, R. Chaplin-Kramer, L. De Meester, E. Dulloo, B. Martín-López, M. R. Shaw, P. Visconti, W. Broadgate, M. W. Bruford, N. D. Burgess, J. Cavender-Bares, F. DeClerck, J. M. Fernández-Palacios, L. A. Garibaldi, S. L. L. Hill, F. Isbell, C. K. Khoury, C. B. Krug, J. Liu, M. Maron, P. J. K. McGowan, H. M. Pereira, V. Reyes-García, J. Rocha, C. Rondinini, L. Shannon, Y.-J. Shin, P. V. R. Snelgrove, E. M. Spehn, B. Strassburg, S. M. Subramanian, J. J. Tewksbury, J. E. M. Watson, A. E. Zanne, Set ambitious goals for biodiversity and sustainability. *Science* **370**, 411–413 (2020). doi:10.1126/science.abe1530 Medline

11. Convention on Biological Diversity (CBD), “First draft of the post-2020 Global Biodiversity Framework” (CBD/WG2020/3/3, United Nations Environment Programme, 2021);

https://www.cbd.int/doc/c/abb5/591f/2e46096d3f0330b08ce87a45/wg2020-03-03-en.pdf.

12. D. M. Leigh, A. P. Hendry, E. Vázquez-Domínguez, V. L. Friesen, Estimated six per cent loss of genetic variation in wild populations since the industrial revolution. *Evol. Appl.* **12**, 1505–1512 (2019). doi:10.1111/eva.12810 Medline

13. K. L. Millette, V. Fugère, C. Debyser, A. Greiner, F. J. J. Chain, A. Gonzalez, No consistent effects of humans on animal genetic diversity worldwide. *Ecol. Lett.* **23**, 55–67 (2020). doi:10.1111/ele.13394 Medline

14. O. Arrhenius, Species and area. *J. Ecol.* **9**, 95–99 (1921). doi:10.2307/2255763

15. D. Storch, P. Keil, W. Jetz, Universal species-area and endemics-area relationships at continental scales. *Nature* **488**, 78–81 (2012). doi:10.1038/nature11226 Medline

16. C. D. Thomas, A. Cameron, R. E. Green, M. Bakkenes, L. J. Beaumont, Y. C. Collingham, B. F. N. Erasmus, M. F. De Siqueira, A. Grainger, L. Hannah, L. Hughes, B. Huntley, A. S. Van Jaarsveld, G. F. Midgley, L. Miles, M. A. Ortega-Huerta, A. T. Peterson, O. L. Phillips, S. E. Williams, Extinction risk from climate change. *Nature* **427**, 145–148 (2004). doi:10.1038/nature02121 Medline

17. V. Buffalo, Quantifying the relationship between genetic diversity and population size suggests natural selection cannot explain Lewontin's Paradox. *eLife* **10**, e67509 (2021). doi:10.7554/eLife.67509 Medline

18. R. A. Fisher, XVII.—The distribution of gene ratios for rare mutations. *Proc. R. Soc. Edinb.* **50**, 204–219 (1931). doi:10.1017/S0370164600044886

19. 1001 Genomes Consortium, 1,135 genomes reveal the global pattern of polymorphism in *Arabidopsis thaliana*. *Cell* **166**, 481–491 (2016). doi:10.1016/j.cell.2016.05.063 Medline

20. F. W. Preston, The canonical distribution of commonness and rarity: Part I. *Ecology* **43**, 185 (1962). doi:10.2307/1931976

21. A. Hampe, R. J. Petit, Conserving biodiversity under climate change: The rear edge matters. *Ecol. Lett.* **8**, 461–467 (2005). doi:10.1111/j.1461-0248.2005.00739.x Medline

22. Millennium Ecosystem Assessment, "Ecosystems and human well-being: Biodiversity synthesis" (World Resources Institute, 2005); https://www.millenniumassessment.org/en/index.html.

23. G. C. Hurtt, L. Chini, R. Sahajpal, S. Frolking, B. L. Bodirsky, K. Calvin, J. C. Doelman, J. Fisk, S. Fujimori, K. Klein Goldewijk, T. Hasegawa, P. Havlik, A. Heinimann, F. Humpenöder, J. Jungclaus, J. O. Kaplan, J. Kennedy, T. Krisztin, D. Lawrence, P. Lawrence, L. Ma, O. Mertz, J. Pongratz, A. Popp, B. Poulter, K. Riahi, E. Shevliakova, E. Stehfest, P. Thornton, F. N. Tubiello, D. P. van Vuuren, X. Zhang, Harmonization of global land use change and management for the period 850–2100 (LUH2) for CMIP6. *Geosci. Model Dev.* **13**, 5425–5464 (2020). doi:10.5194/gmd-13-5425-2020

24. International Union for Conservation of Nature (IUCN), "Guidelines for using the IUCN Red List categories and criteria," version 15 (IUCN, 2022); https://www.iucnredlist.org/resources/redlistguidelines.

25. R. P. Powers, W. Jetz, Global habitat loss and extinction risk of terrestrial vertebrates under future land-use-change scenarios. *Nat. Clim. Chang.* **9**, 323–329 (2019). doi:10.1038/s41558-019-0406-z

26. D. L. Halligan, P. D. Keightley, Spontaneous mutation accumulation studies in evolutionary genetics. *Annu. Rev. Ecol. Evol. Syst.* **40**, 151–172 (2009). doi:10.1146/annurev.ecolsys.39.110707.173437

27. M. V. Rockman, The QTN program and the alleles that matter for evolution: All that's gold does not glitter. *Evolution* **66**, 1–17 (2012). doi:10.1111/j.1558-5646.2011.01486.x Medline

28. M. J. Harms, J. W. Thornton, Evolutionary biochemistry: Revealing the historical and physical causes of protein properties. *Nat. Rev. Genet.* **14**, 559–571 (2013). doi:10.1038/nrg3540 Medline

29. M. Exposito-Alonso, H. A. Burbano, O. Bossdorf, R. Nielsen, D. Weigel, 500 Genomes Field Experiment Team, Natural selection on the *Arabidopsis thaliana* genome in present and future climates. *Nature* **573**, 126–129 (2019). doi:10.1038/s41586-019-1520-9 Medline

30. H. R. Taft, D. A. Roff, Do bottlenecks increase additive genetic variance? *Conserv. Genet.* **13**, 333–342 (2012). doi:10.1007/s10592-011-0285-y

31. P. Ehrlich, B. Walker, Rivets and redundancy. *Bioscience* **48**, 387 (1998). doi:10.2307/1313377

32. M. Kardos, E. E. Armstrong, S. W. Fitzpatrick, S. Hauser, P. W. Hedrick, J. M. Miller, D. A. Tallmon, W. C. Funk, The crucial role of genome-wide genetic variation in conservation. *Proc. Natl. Acad. Sci. U.S.A.* **118**, e2104642118 (2021). doi:10.1073/pnas.2104642118 Medline

33. M. Exposito-Alonso, Scripts to build the mutations area relationship. Zenodo (2022); https://doi.org/10.5281/zenodo.6408624.

34. S. P. Hubbell, *The Unified Neutral Theory of Biodiversity and Biogeography* (Monographs in Population Biology Series, Princeton Univ. Press, 2001).

35. M. Tokeshi, Niche apportionment or random assortment: Species abundance patterns revisited. *J. Anim. Ecol.* **59**, 1129–1146 (1990). doi:10.2307/5036

36. M. Tokeshi, in *Advances in Ecological Research*, vol. 24, M. Begon, A. H. Fitter, Eds. (Academic Press, 1993), pp. 111–186.

37. R. A. Fisher, A. S. Corbet, C. B. Williams, The relation between the number of species and the number of individuals in a random sample of an animal population. *J. Anim. Ecol.* **12**, 42–58 (1943). doi:10.2307/1411

38. F. W. Preston, The commonness, and rarity, of species. *Ecology* **29**, 254–283 (1948). doi:10.2307/1930989

39. D. Alonso, A. J. McKane, Sampling Hubbell's neutral theory of biodiversity. *Ecol. Lett.* **7**, 901–910 (2004). doi:10.1111/j.1461-0248.2004.00640.x

40. S. L. Pimm, G. J. Russell, J. L. Gittleman, T. M. Brooks, The future of biodiversity. *Science* **269**, 347–350 (1995). doi:10.1126/science.269.5222.347 Medline

41. J. F. C. Kingman, The coalescent. *Stochastic Process. Appl.* **13**, 235–248 (1982). doi:10.1016/0304-4149(82)90011-4

42. R. C. Griffiths, S. Tavaré, The age of a mutation in a general coalescent tree. *Commun. Stat. Stoch. Models* **14**, 273–295 (1998). doi:10.1080/15326349808807471

43. M. W. Hahn, *Molecular Population Genetics* (Oxford Univ. Press, 2018).

44. D. R. Marshal, A. D. H. Brown, in *Crop Genetic Resources for Today and Tomorrow*, vol. 2, O. H. Frankel, J. G. Hawkes, Eds. (Cambridge Univ. Press, 1975).

45. S. Wright, Isolation by distance. *Genetics* **28**, 114–138 (1943). doi:10.1093/genetics/28.2.114 Medline

46. J. Novembre, M. Stephens, Interpreting principal component analyses of spatial population genetic variation. *Nat. Genet.* **40**, 646–649 (2008). doi:10.1038/ng.139 Medline

47. H. Fan, Q. Zhang, J. Rao, J. Cao, X. Lu, Genetic diversity-area relationships across bird species. *Am. Nat.* **194**, 736–740 (2019). doi:10.1086/705346

48. P. R. A. Campos, V. M. de Oliveira, A. Rosas, Epistasis and environmental heterogeneity in the speciation process. *Ecol. Modell.* **221**, 2546–2554 (2010). doi:10.1016/j.ecolmodel.2010.07.023

49. J. Kelleher, A. M. Etheridge, G. McVean, Efficient coalescent simulation and genealogical analysis for large sample sizes. *PLOS Comput. Biol.* **12**, e1004842 (2016). doi:10.1371/journal.pcbi.1004842 Medline

50. B. C. Haller, P. W. Messer, SLiM 3: Forward genetic simulations beyond the Wright-Fisher model. *Mol. Biol. Evol.* **36**, 632–637 (2019). doi:10.1093/molbev/msy228 Medline

51. T. R. Booker, S. Yeaman, M. C. Whitlock, The WZA: A window-based method for characterizing genotype-environment association. bioRxiv 2021.06.25.449972 [Preprint] (2021); https://doi.org/10.1101/2021.06.25.449972.

52. J. Kelleher, K. R. Thornton, J. Ashander, P. L. Ralph, Efficient pedigree recording for fast population genetics simulation. *PLOS Comput. Biol.* **14**, e1006581 (2018). doi:10.1371/journal.pcbi.1006581 Medline

53. B. C. Haller, J. Galloway, J. Kelleher, P. W. Messer, P. L. Ralph, Tree-sequence recording in SLiM opens new horizons for forward-time simulation of whole genomes. *Mol. Ecol. Resour.* **19**, 552–566 (2019). doi:10.1111/1755-0998.12968 Medline

54. R. R. Hudson, M. Slatkin, W. P. Maddison, Estimation of levels of gene flow from DNA sequence data. *Genetics* **132**, 583–589 (1992). doi:10.1093/genetics/132.2.583 Medline

55. H. M. Pereira, G. C. Daily, Modeling biodiversity dynamics in countryside landscapes. *Ecology* **87**, 1877–1885 (2006). doi:10.1890/0012-9658(2006)87[1877:MBDICL]2.0.CO;2 Medline

56. H. M. Pereira, G. Ziv, M. Miranda, Countryside species-area relationship as a valid alternative to the matrix-calibrated species-area model. *Conserv. Biol.* **28**, 874–876 (2014). doi:10.1111/cobi.12289 Medline

57. J. Gallego-Zamorano, M. A. J. Huijbregts, A. M. Schipper, Changes in plant species richness due to land use and nitrogen deposition across the globe. *Divers. Distrib.* **28**, 745–755 (2022). doi:10.1111/ddi.13476

58. B. J. McGill, B. J. Enquist, E. Weiher, M. Westoby, Rebuilding community ecology from functional traits. *Trends Ecol. Evol.* **21**, 178–185 (2006). doi:10.1016/j.tree.2006.02.002 Medline

59. P. I. Prado, M. Miranda, A. Chalom, sads: R package for fitting species abundance distributions, Github (2018); https://github.com/piLaboratory/sads.

60. T. J. Matthews, K. A. Triantis, R. J. Whittaker, F. Guilhaumon, sars: An R package for fitting, evaluating and comparing species–area relationship models. *Ecography* **42**, 1446–1455 (2019). doi:10.1111/ecog.04271

61. F. He, S. P. Hubbell, Species-area relationships always overestimate extinction rates from habitat loss. *Nature* **473**, 368–371 (2011). doi:10.1038/nature09985 Medline

62. J. Hijmans, raster: Geographic data analysis and modeling (2012); http://CRAN.R-project.org/package=raster.

63. Y. B. Simons, K. Bullaughey, R. R. Hudson, G. Sella, A population genetic interpretation of GWAS findings for human quantitative traits. *PLOS Biol.* **16**, e2002985 (2018). doi:10.1371/journal.pbio.2002985 Medline

64. M. Exposito-Alonso, C. Becker, V. J. Schuenemann, E. Reiter, C. Setzer, R. Slovak, B. Brachi, J. Hagmann, D. G. Grimm, J. Chen, W. Busch, J. Bergelson, R. W. Ness, J. Krause, H. A. Burbano, D. Weigel, The rate and potential relevance of new mutations in a colonizing plant lineage. *PLOS Genet.* **14**, e1007155 (2018). doi:10.1371/journal.pgen.1007155 Medline

65. H. Seebens, T. M. Blackburn, E. E. Dyer, P. Genovesi, P. E. Hulme, J. M. Jeschke, S. Pagad, P. Pyšek, M. Winter, M. Arianoutsou, S. Bacher, B. Blasius, G. Brundu, C. Capinha, L. Celesti-Grapow, W. Dawson, S. Dullinger, N. Fuentes, H. Jäger, J. Kartesz, M. Kenis, H. Kreft, I. Kühn, B. Lenzner, A. Liebhold, A. Mosena, D. Moser, M. Nishino, D. Pearman, J. Pergl, W. Rabitsch, J. Rojas-Sandoval, A. Roques, S. Rorke, S. Rossinelli, H. E. Roy, R. Scalera, S. Schindler, K. Štajerová, B. Tokarska-Guzik, M. van Kleunen, K. Walker, P. Weigelt, T. Yamanaka, F. Essl, No saturation in the accumulation of alien species worldwide. *Nat. Commun.* **8**, 14435 (2017). doi:10.1038/ncomms14435 Medline

66. H. Seebens, F. Essl, W. Dawson, N. Fuentes, D. Moser, J. Pergl, P. Pyšek, M. van Kleunen, E. Weber, M. Winter, B. Blasius, Global trade will accelerate plant invasions in emerging economies under climate change. *Glob. Change Biol.* **21**, 4128–4140 (2015). doi:10.1111/gcb.13021 Medline

67. S. Purcell, B. Neale, K. Todd-Brown, L. Thomas, M. A. R. Ferreira, D. Bender, J. Maller, P. Sklar, P. I. W. de Bakker, M. J. Daly, P. C. Sham, PLINK: A tool set for whole-genome association and population-based linkage analyses. *Am. J. Hum. Genet.* **81**, 559–575 (2007). doi:10.1086/519795 Medline

68. C. Mérot, R. A. Oomen, A. Tigano, M. Wellenreuther, A roadmap for understanding the evolutionary significance of structural genomic variation. *Trends Ecol. Evol.* **35**, 561–572 (2020). doi:10.1016/j.tree.2020.03.002 Medline

69. K. Lucek, Y. Willi, Drivers of linkage disequilibrium across a species' geographic range. *PLOS Genet.* **17**, e1009477 (2021). doi:10.1371/journal.pgen.1009477 Medline

70. J. M. Kreiner, D. A. Giacomini, F. Bemm, B. Waithaka, J. Regalado, C. Lanz, J. Hildebrandt, P. H. Sikkema, P. J. Tranel, D. Weigel, J. R. Stinchcombe, S. I. Wright, Multiple modes of convergent adaptation in the spread of glyphosate-resistant

Amaranthus tuberculatus. *Proc. Natl. Acad. Sci. U.S.A.* **116**, 21076–21084 (2019). doi:10.1073/pnas.1900870116 Medline

71. M. A. Supple, J. G. Bragg, L. M. Broadhurst, A. B. Nicotra, M. Byrne, R. L. Andrew, A. Widdup, N. C. Aitken, J. O. Borevitz, Landscape genomic prediction for restoration of a *Eucalyptus* foundation species under climate change. *eLife* **7**, e31835 (2018). doi:10.7554/eLife.31835 Medline

72. M. Vallejo-Marín, J. Friedman, A. D. Twyford, O. Lepais, S. M. Ickert-Bond, M. A. Streisfeld, L. Yant, M. van Kleunen, M. C. Rotter, J. R. Puzey, Population genomic and historical analysis suggests a global invasion by bridgehead processes in *Mimulus guttatus*. *Commun. Biol.* **4**, 327 (2021). doi:10.1038/s42003-021-01795-x Medline

73. J. T. Lovell, A. H. MacQueen, S. Mamidi, J. Bonnette, J. Jenkins, J. D. Napier, A. Sreedasyam, A. Healey, A. Session, S. Shu, K. Barry, S. Bonos, L. Boston, C. Daum, S. Deshpande, A. Ewing, P. P. Grabowski, T. Haque, M. Harrison, J. Jiang, D. Kudrna, A. Lipzen, T. H. Pendergast IV, C. Plott, P. Qi, C. A. Saski, E. V. Shakirov, D. Sims, M. Sharma, R. Sharma, A. Stewart, V. R. Singan, Y. Tang, S. Thibivillier, J. Webber, X. Weng, M. Williams, G. A. Wu, Y. Yoshinaga, M. Zane, L. Zhang, J. Zhang, K. D. Behrman, A. R. Boe, P. A. Fay, F. B. Fritschi, J. D. Jastrow, J. Lloyd-Reilley, J. M. Martínez-Reyna, R. Matamala, R. B. Mitchell, F. M. Rouquette Jr., P. Ronald, M. Saha, C. M. Tobias, M. Udvardi, R. A. Wing, Y. Wu, L. E. Bartley, M. Casler, K. M. Devos, D. B. Lowry, D. S. Rokhsar, J. Grimwood, T. E. Juenger, J. Schmutz, Genomic mechanisms of climate adaptation in polyploid bioenergy switchgrass. *Nature* **590**, 438–444 (2021). doi:10.1038/s41586-020-03127-1 Medline

74. I. R. MacLachlan, T. K. McDonald, B. M. Lind, L. H. Rieseberg, S. Yeaman, S. N. Aitken, Genome-wide shifts in climate-related variation underpin responses to selective breeding in a widespread conifer. *Proc. Natl. Acad. Sci. U.S.A.* **118**, e2016900118 (2021). doi:10.1073/pnas.2016900118 Medline

75. G. Tuskan, W. Muchero, J.-G. Chen, D. Jacobson, T. Tschaplinski, D. Rokhsar, W. Schackwitz, J. Schmutz, S. DiFazio, *Populus trichocarpa* genome-wide association study (GWAS) population SNP dataset released, Oak Ridge National Laboratory, Leadership Computing Facility (2017); https://doi.org/10.13139/OLCF/1411410.

76. The *Anopheles gambiae* 1000 Genomes Consortium, Genetic diversity of the African malaria vector *Anopheles gambiae*. *Nature* **552**, 96–100 (2017). doi:10.1038/nature24995 Medline

77. Z. L. Fuller, V. J. L. Mocellin, L. A. Morris, N. Cantin, J. Shepherd, L. Sarre, J. Peng, Y. Liao, J. Pickrell, P. Andolfatto, M. Matz, L. K. Bay, M. Przeworski, Population genetics of the coral *Acropora millepora*: Toward genomic prediction of bleaching. *Science* **369**, eaba4674 (2020). doi:10.1126/science.aba4674 Medline

78. K. Ruegg, E. C. Anderson, M. Somveille, R. A. Bay, M. Whitfield, E. H. Paxton, T. B. Smith, Linking climate niches across seasons to assess population vulnerability in a migratory bird. *Glob. Change Biol.* **27**, 3519–3531 (2021). doi:10.1111/gcb.15639 Medline

79. R. A. Bay, R. J. Harrigan, V. L. Underwood, H. L. Gibbs, T. B. Smith, K. Ruegg, Genomic signals of selection predict climate-driven population declines in a migratory bird. *Science* **359**, 83–86 (2018). doi:10.1126/science.aan4380 Medline

80. E. P. Kingsley, K. M. Kozak, S. P. Pfeifer, D.-S. Yang, H. E. Hoekstra, The ultimate and proximate mechanisms driving the evolution of long tails in forest deer mice. *Evolution* **71**, 261–273 (2017). doi:10.1111/evo.13150 Medline

81. L. Smeds, J. Aspi, J. Berglund, I. Kojola, K. Tirronen, H. Ellegren, Whole-genome analyses provide no evidence for dog introgression in Fennoscandian wolf populations. *Evol. Appl.* **14**, 721–734 (2020). doi:10.1111/eva.13151 Medline

82. R. M. Schweizer, J. Robinson, R. Harrigan, P. Silva, M. Galverni, M. Musiani, R. E. Green, J. Novembre, R. K. Wayne, Targeted capture and resequencing of 1040 genes reveal environmentally driven functional variation in grey wolves. *Mol. Ecol.* **25**, 357–379 (2016). doi:10.1111/mec.13467 Medline

83. 1000 Genomes Project Consortium, A. Auton, L. D. Brooks, R. M. Durbin, E. P. Garrison, H. M. Kang, J. O. Korbel, J. L. Marchini, S. McCarthy, G. A. McVean, G. R. Abecasis, A global reference for human genetic variation. *Nature* **526**, 68–74 (2015). doi:10.1038/nature15393 Medline

84. J. D. Palacio-Mejía, P. P. Grabowski, E. M. Ortiz, G. A. Silva-Arias, T. Haque, D. L. Des Marais, J. Bonnette, D. B. Lowry, T. E. Juenger, Geographic patterns of genomic diversity and structure in the C_4 grass *Panicum hallii* across its natural distribution. *AoB Plants* **13**, plab002 (2021). doi:10.1093/aobpla/plab002 Medline

85. A. M. Royer, M. A. Streisfeld, C. I. Smith, Population genomics of divergence within an obligate pollination mutualism: Selection maintains differences between Joshua tree species. *Am. J. Bot.* **103**, 1730–1741 (2016). doi:10.3732/ajb.1600069 Medline

86. M. Kapun, J. C. B. Nunez, M. Bogaerts-Márquez, J. Murga-Moreno, M. Paris, J. Outten, M. Coronado-Zamora, C. Tern, O. Rota-Stabelli, M. P. G. Guerreiro, S. Casillas, D. J. Orengo, E. Puerma, M. Kankare, L. Ometto, V. Loeschcke, B. S. Onder, J. K. Abbott, S. W. Schaeffer, S. Rajpurohit, E. L. Behrman, M. F. Schou, T. J. S. Merritt, B. P. Lazzaro, A. Glaser-Schmitt, E. Argyridou, F. Staubach, Y. Wang, E. Tauber, S. V. Serga, D. K. Fabian, K. A. Dyer, C. W. Wheat, J. Parsch, S. Grath, M. S. Veselinovic, M. Stamenkovic-Radak, M. Jelic, A. J. Buendía-Ruíz, M. J. Gómez-Julián, M. L. Espinosa-Jimenez, F. D. Gallardo-Jiménez, A. Patenkovic, K. Eric, M. Tanaskovic, A. Ullastres, L. Guio, M. Merenciano, S. Guirao-Rico, V. Horváth, D. J. Obbard, E. Pasyukova, V. E. Alatortsev, C. P. Vieira, J. Vieira, J. R. Torres, I. Kozeretska, O. M. Maistrenko, C. Montchamp-Moreau, D. V. Mukha, H. E. Machado, K. Lamb, T. Paulo, L. Yusuf, A. Barbadilla, D. Petrov, P. Schmidt, J. Gonzalez, T. Flatt, A. O. Bergland, Drosophila Evolution over Space and Time (DEST): A new population genomics resource. *Mol. Biol. Evol.* **38**, 5782–5805 (2021). doi:10.1093/molbev/msab259 Medline

87. L. N. Di Santo, S. Hoban, T. L. Parchman, J. W. Wright, J. A. Hamilton, Reduced representation sequencing to understand the evolutionary history of Torrey pine (Pinus torreyana Parry) with implications for rare species conservation. *bioRxiv* (2021), p. 2021.07.02.450939.

88. J. von Seth, N. Dussex, D. Díez-Del-Molino, T. van der Valk, V. E. Kutschera, M. Kierczak, C. C. Steiner, S. Liu, M. T. P. Gilbert, M. S. Sinding, S. Prost, K. Guschanski, S. K. S. S. Nathan, S. Brace, Y. L. Chan, C. W. Wheat, P. Skoglund, O. A. Ryder, B. Goossens, A. Götherström, L. Dalén, Genomic insights into the conservation status of the world's last remaining Sumatran rhinoceros populations. *Nat. Commun.* **12**, 2393 (2021). doi:10.1038/s41467-021-22386-8 Medline

89. S. Theodoridis, C. Rahbek, D. Nogues-Bravo, Exposure of mammal genetic diversity to mid-21st century global change. *Ecography* **44**, 817–831 (2021). doi:10.1111/ecog.05588

90. I. Overcast, M. Ruffley, J. Rosindell, L. Harmon, P. A. V. Borges, B. C. Emerson, R. S. Etienne, R. Gillespie, H. Krehenwinkel, D. L. Mahler, F. Massol, C. E. Parent, J. Patiño, B. Peter, B. Week, C. Wagner, M. J. Hickerson, A. Rominger, A unified model of species abundance, genetic diversity, and functional diversity reveals the mechanisms structuring ecological communities. *Mol. Ecol. Resour.* **21**, 2782–2800 (2021). doi:10.1111/1755-0998.13514 Medline